Electronic Thesis and Dissertation Repository

2-14-2022 2:30 PM

Erosion Control of Steep Open Channels Using Articulated Concrete Blocks

MohammadOmid Marandi, *The University of Western Ontario*

Supervisor: Najafi, Mohammad Reza, *The University of Western Ontario*
Co-Supervisor: Sadrekarimi, Abouzar, *The University of Western Ontario*
A thesis submitted in partial fulfillment of the requirements for the Master of Engineering
Science degree in Civil and Environmental Engineering
© MohammadOmid Marandi 2022

Abstract

Overtopping flow can undermine the stability of hydraulic structures including embankments and spillways through the shear stress and the subsequent soil erosion. Increased flow velocity can cause scour, which can result in the failure of dams, bridges, and overall open channel hydraulic structures. Sediment transport is another crucial issue in open channels that can cause severe socioeconomic and environmental consequences. Two general approaches are commonly considered for scour prevention. The first approach involves flow modifications to minimize the corresponding effects on the structures. The second approach is associated with bed armoring and placing physical barriers on the natural bedding such as the Articulated Concrete Block system (ACBs).

The Articulated Concrete Block (ACB) system includes a series of concrete blocks or slabs that are interconnected using steel or synthetic cables, which are commonly employed for the bed and bank protection of open channels. Two flow-induced failure mechanisms can undermine the performance of ACBs: Direct failure, which is attributed to the direct impact of free-surface flow on concrete blocks leading to the overturning or rolling-up of the edge of the ACB. Indirect failure is associated with the scouring of the underlying bedding that can result in the deformation of the ACB structure and its failure. The main objective of this study is to analyze the ACBs protection layer, understand the factors that can influence scouring, and develop measures to reduce the failure risks and minimize the amount of sediment transport of the bedding and the subgrade. The indirect failure mechanisms of ACBs laid over the downstream face of an embankment are explored through a suite of laboratory experiments (∼ 40 tests). The effects of substrate structure, soil particle size, the slope of the embankment, and different types of permeable filters (i.e., geotextile, geogrid, and filter cloth mats) on the incipient motion of the bedding and the amount of soil loss are assessed. The stability of the embankment is investigated through various configurations with different water depths and velocities. Results show that overtopping flow with high velocity causes soil erosion and sediment transport in a very short period of time with the absence of a protection layer. ACB

can noticeably improve channel stability and reduce sediment transport due to its perfect contact with subgrade and its flexibility. However, the risk of ACB failure increases if the subgrade is not designed and implemented properly. ACBs are to be in close contact with the subgrade and the fabrics and spaces between the blocks should be optimized otherwise, the overtopping of the blocks and sediment transport happen. The fabrics placed in between the layers can prevent the suction of the finer particles and reduce the risk of failure. Coarser and well-grade particles underneath the ACB structure can drain more water due to their higher hydraulic conductivity and improve the stability of the embankment. Further, risks of failure are higher near the downstream toe, which can be partly controlled by sufficient flow drainage and anchoring the downstream segments. The subgrade beneath the ACB is to be uniformly compacted so that the water flow passes through the blocks and over the subgrade steadily. The median diameter and the slope of the embankment played a key role in mitigating the amount of soil loss.

Summary for Lay Audience

As rainfall washes away bare soil or a stream erodes a muddy bank, sediment makes its way into the waterways. Fine suspended particles cause turbidity in waterways, making the water less transparent by blocking sunlight. The decreased light will deteriorate the growth of aquatic plants, which provide essential habitat for many aquatic animals, including young fish.

In addition to its effects on aquatic plants and animals, sediment can fill streams, lakes, and ponds, obstruct waterways and clog storm sewers and ditches. Sediment deposits in rivers can alter the flow of water and reduce water depth making navigation and recreational use more difficult. Morphological changes (physical changes over a large area) to large aquatic systems can also result in major changes in natural sediment erosion and sedimentation patterns. As an example, the change in the size and shape of a water body will result in new water flow patterns leading to erosion or sediment removal from sensitive areas. Many marine environmental indicators show that the sea in many parts of the world, especially in coastal areas, is at high risk.

Scouring occurs when fast-moving overtopping flow of water over an embankment or the water flow around a bridge or embankments removes sediment from the streambed, leaving behind scour holes below the foundations. These holes can seriously damage the structure and affect the functionality. Some of the fundamental elements of these hydraulic structures can hardly be seen such as abutments and footings submerged under the waterline. Hydraulic open channels structures failures cost millions of dollars each year in direct expenditure for replacement and restoration in addition to the indirect expenditure related to the disruption of transportation facilities. A series of failures due to soil wash and soil erosion, as reported during floods, has rekindled interest in our understanding of the scouring process and for developing improved ways of protecting the structures against scour. As such, attention is being given to the scour preventive measures to minimize the amount of soil loss and sediment transport.

There are some countermeasure techniques that could be used for preventing or minimizing local scour on embankments, culverts, spillways, etc., including ripraps and Artic-

ulated Concrete Blocks. Articulated Concrete Blocks consist of an interconnected matrix of concrete block units (hard-armor products) with hydraulic performance characteristics placed across the channel that is commonly used for scour prevention. ACBs systems are used to provide erosion protection to underlying soil from the hydraulic forces of moving water. The stability of the protection layer depends on different configurations, subgrade characteristics, the thickness of the layers, flow depth, etc. In this study, I conducted a large set of experiments to assess the underlying bed strength, which has been mostly neglected in the ACB design, and to find the best configuration to reach the desired protection strength.

Acknowledgment

First and foremost, I would like to thank my supervisor, Dr. Mohammad Reza Najafi, for his guidance and patient support that helped me throughout this research. His constructive guidance and consistent support helped me get this far and brought my work to a higher level. I am also highly grateful for all of his hard work and insightful feedback that has kept me moving forward and completing this dissertation.

I would also like to thank my co-supervisor, Dr. Abouzar Sadrekarimi, for his valuable guidance and support throughout my studies. Also, I would like to acknowledge Dr. Jalal Attari, Dr. Hossein Mohajeri, Dr. Tim Newson, and Dr. Aly Ahmed for their constructive criticisms and ideas that helped me choose the right direction toward completing my dissertation.

A special thanks goes to Mr. Louis Arvai, Greg Arvai, David Talan, and the IECS members for providing me with the experiments facilities, site visit opportunities, and their creative ideas toward my research goals.

I have been fortunate to meet and work with a number of helpful and talented individuals during my time at Western University. In particular, I would like to thank Soheil Bakhtiari, Navid Feizi, Farzad Poodeh, Zahra Habibollahi, Payam Momeni, Afshin Marani, and Aiham Adawi.

This research is dedicated to my lovely parents, Azita and Mohammad, whose all-time dedications for me are absolutely unforgettable. I would always be thankful for the rest of my life.

Table of Contents

List of Tables

List of Figures

ACB: Articulated Concrete Block

Embankment: a raised confining structure made from wood to provide overtopping flow

Broad Crested Weir: a hydraulic structure which is widely used for depth control and flow measurement in fields and laboratories

Winnowing: removal of fine material from coarser sediment by flowing water

Scouring: removal of materials from beds and banks of streams

Sediment transport: movement of the soil particles due to the movement of the water flow

Hydraulic conductivity: saturated soil's ability to transmit water when subjected to hydraulic gradient

Q: maximum rate of water flow $\left(\frac{M}{L^3}\right)$

H: water depth(L)

t: the thickness of the layers(L)

V: velocity$\left(\frac{L}{T}\right)$

D_{50}**:** median diameter of the soil particles

δ**:** the amount of the subgrade soil loss in each experiment (L^3)

θ_c**:** critical shear stress applied by hydraulic forces

s: the slope of the embankment

g: gravitational acceleration$\left(\frac{L}{T^2}\right)$

Chapter 1

Thesis Overview

The two major countermeasure techniques that are commonly used for preventing or minimizing local scour at embankments, levees, and spillways include riprap and Articulated Concrete Block systems. Ripraps are not always accessible and suitable for steep slopes and there are some certain failures that happen in between their gaps such as winnowing, and edge failure which may happen due to lack of adequate support along the surface. One of the effective approaches to prevent scouring is Articulated Concrete Block which is made of an interconnected matrix of concrete block units (hard-armor products) placed across the channel. ACBs have been implemented to stabilize spillways, culvert inlet/outlet, riverbank protection, and bank revetement. ACB systems are used to provide erosion protection to underlying soil from the hydraulic forces of overflows (Nemry et al., 2012; Maddison, 2012). This research is aimed at obtaining a better understanding of the underlying bed strength based on 40 laboratory experiments analyzing the indirect failure of the cable concrete blocks to find the optimal configuration for a reliable ACB implementation.

1.1 RESEARCH OBJECTIVES

The overall objective of this study is to assess the effectiveness of subgrade configuration underneath the Articulated Concrete Blocks through a suite of laboratory experiments. The durability and stability of the corresponding mat systems depend on several hydraulic and soil components. The sub-objectives of this research are as follows:

- Recognize the influential parameters that affect the local erosion along the channel segments.

- Identify the optimal subgrade configuration to stabilize the bedding for the protec-

tive layer.

- Assess the individual influence of subgrade parameters in the failure and stability of the ACBs.

Multiple influential variables have been considered and assessed in the experiments to comprehend their effectiveness for scour prevention and to find the stability threshold conditions. The performance threshold for the ACB system can be defined as the point in which deformation, soil loss, or loss of intimate contact with the embankment subgrade occurred.

1.2 Research Questions

The following questions will be addressed in this study:

- what are the influential failure mechanisms?

- what is the optimal particle soil size for the subgrade configuration?

- What types of fabric layers work best (against scour) with underlying sand and gravel, respectively?

- How do various subgrade configurations behave under different channel slopes?

1.3 Summary of Chapters

This thesis is based on four main chapters. Chapter 1 of this thesis includes a brief background of the thesis and the objectives of this study.
The first part of chapter 2 of this thesis includes an overview of the previous studies related to sediment transport and scouring mostly for embankments, and the shape of the scourings. The second section of this chapter describes the experiments and the studies conducted using scour protection layers using the riprap and granular filter layer and their limitations. Further, the experiments and studies conducted so far on Articulated Concrete Block systems are presented.

Chapter 3 describes the methodology, the laboratory experimental procedure in the hydraulics lab at Western University, and all the details of the tests setups. Moreover, various materials and configurations for the 40 experiments are discussed.

Chapter 4 presents the results of the findings of the laboratory experiments and the effect of the dominant variables affecting the stability of the ACBs.

Bibliography

Maddison, B. (2012). Scour failure of bridges. *Proceedings of the Institution of Civil Engineers-Forensic Engineering*, 165(1):39–52.

Nemry, F., Demirel, H., et al. (2012). Impacts of climate change on transport: A focus on road and rail transport infrastructures. *European Commission, Joint Research Centre (JRC), Institute for Prospective Technological Studies (IPTS)*.

Chapter 2

Introduction

2.1 SEDIMENT

Sediment transport in supercritical open channel flows occurs mostly in higher gradient mountain streams and over hydraulic structures such as spillways, and weirs. This can result in a considerable annual maintenance cost for these kinds of structures (Auel et al., 2017). Sedimentation can affect agricultural practices, water quality, aquatic habitat, and pollutants. It can affect the river morphology and the river bank stability. There are some influential factors in sediment transport such as grain size. Finer materials such as silt and clay are transported easier as they enter the channel. In terms of the grain distribution, grading instability, which is one of the key factors in the grain size of the sediments, is most likely to occur in soils that have a slope with a wide range of particle sizes in the lower part of their grading curves. Grading stability is related to size and particles distribution, porosity, and intensity of the forces and can significantly affect the amount of sediment transport (Kenney and Lau, 1985). Sedimentation equilibrium is another factor regarding the amount of sediment transported; Should the sediments input in a channel be equivalent to the output it is called equilibrium. when the sediment coming out of a channel is greater than the sediment coming in, degradation happens (particularly during the flood) and it results in some changes in the geomorphology of the river channel.

Sediment particles transport happens in different forms, rolling which happens in low flow velocity, saltation, and suspended form. Particles in rolling, sliding, or saltation mode are considered as bed load. Auel et al. (2014) conducted an experiment to determine the bedload particle velocity in supercritical flow in a laboratory flume and found that large particles move roughly 5% faster than small ones and particles transported in saltation mode move faster than those of rolling mode. Normalized particle velocity increases with

5

Froude number from subcritical to supercritical and it is a function of the shear velocity as well.

2.2 SCOURING

Hydraulic structures change the local flow pattern, which can lead to local erosion (scouring) and transport of sediments. Scour can be defined as the removal of granular materials by hydrodynamic forces and occurs when hydrodynamic bottom shear stress is greater than sediment critical shear stress. Surface erosion is the removal of soil particles due to the velocity and turbulence of the surface flow. Scour is the result of increased velocities and shear stress on the channel bed. Live-bed scouring happens when the amount of sediment out of the scour hole equals the amount into the hole. Local scour involves the removal of material around piers and abutment, which is caused by an acceleration of flow and resulting vortices induced by the flow obstruction (Lagasse, 2007). The effect and the mechanism of scouring on different structures have been analyzed in previous studies (Delgado-Ramos et al., 2012; Zomorodian and Moghadam, 2011; Amaral et al.).

The internal stability of granular material is the corresponding capability to prevent loss of fine particles which may lead to scouring. Shear failure is one of the noticeable factors in the failure mechanism in which the stones start to move resulting in erosion (Joustra, 2013). In non-cohesive material particle weight as well as its grain size distribution plays a role in the resistance of the particle against erosion.

In addition to the gran sizes, soil characteristics and hydraulic features may affect the scour mechanism. For cohesive material, Delgado-Ramos et al. (2012) studied base soil filter systems in embankments and conducted experiments in perspex cylinders. They found that plasticity and mineralogy have no effect on the results and embankments with clay core are to be compacted at the optimum water content and higher density otherwise they are more likely to be eroded. Zomorodian and Moghadam (2011) studied the effects of the cracking in the core of the embankment and found out that there is a relation between materials erosion and hydraulic gradient.
Materials are considered stable if they do not lose particles. Dargahi (2003) conducted experiments to evaluate the scouring mechanisms downstream of a spillway after a protection plate with two different soil types. The generated hydraulic jump downstream of the spillway played a key role in forming the clockwise vortices that created scouring. By adding extra roughness to the protection plate, flow remained unchanged yet scour cavities decreased.

As overtopping accounts for a large proportion of levee and dam failures, it is crucial to understand the corresponding mechanisms and develop effective preventive control measures. When erosion initiates, the cavities and vortices increase in size followed by a higher volume of flow which leads to failure of the system. Hydraulic erodibility can be characterized by soil erosion resistance and the amount of erosion. For clayey core soils, the erosion initiates from the dam toe and moves towards the upstream of the slope. In terms of homogeneous earthfill dames, Amaral et al.(2020) studied dam morphology, flow kinematics, erosion mechanism, and time scales of dam failure. Failure of embankment dams on sandy soils and clayey sand exposed to overtopping flow were analyzed through some experiments. Vibration, low-weight vibratory plate, and lawn roller were used as different compaction methods. They came up with some results as such, grain size distribution is to be coarser than the geometric scaling and compaction method should be different with the prototype as well as lawn roller as an instance showed to be inappropriate due to its compaction capabilities just close to the surface of the embankment and percussion showed to be more suitable for the soil used in their study. Low compaction as well as drier soil particles showed the worst scenario and ends in the minimum shear resistance and increased erodibility. Erosion of the soil happens as the shear stress occurs by flowing water and larger particle and well-graded soil was recommended and showed more stability against water flow.

Scouring in culverts, embankments, and around bridge piers can cause millions of dollars in damage due to the replacement and renovation of both direct and indirect destructive effects. Rasaei et al. (2020) studied the effects of the shape of piers (both cylindrical and cubic) with different angles on scouring around bridge piers. Depth of the scour placed around cylindrical was lower compared with the ones around cubic piers. As the angle increased the scouring depth around the piers was increased. The shape of the piers of bridges has a considerable effect on scouring effects and depth, particularly in deeper flows. The elliptical shape shows the minimum scour depth compared with diamond and rounded shape piers, whereas the diamond shape shows the maximum scour depth (PASHA et al.).

Dargahi (1990) studied the mechanisms of scouring near piers, which consist of horseshoe and wake vortices. The first vortex lifts up and traps the sediment afterward and upcoming vortices will deposit the particle. This process continues back and forth until scour and deposition happen. The scouring process includes different steps, beginning during which the change in bedding is not significant, the main scouring which the vortices gradually makes the profiles of scouring and moderate particle loss. Placing collars

with various shapes was suggested as a method for decreasing scouring. Locations of the collars at a certain distance of the bed may decrease the scour depth, but neither of them can prevent the scour and horseshoe vortices.

To understand the effects of scouring and better control and mitigate its progress, empirical equations are developed/applied. Nadal and Hughes (2009) derived new empirical equations based on combined wave and surge over an earthen grass-covered levee with different wave heights and flow thicknesses. Weibull distribution parameters were studied and horizontal velocity, as well as water elevation, were recorded to estimate the time series of overtopping discharge. Some empirical equations were found out for different sections of the embankment, as such, average overtopping discharge per unit length along with the setup crest as a function of negative freeboard and incident energy-based significant wave height. The shear stress equation could help minimize and regulate the effect of key variables that affect the scouring.

2.3 Protective layers

Protective layers such as granular filters, stone, and High-Performance Turf Reinforcement Mats (HPTRM) are commonly used to protect channel beds against scouring. Filters, as cover layers, provide adequate strength against the hydraulic shear stress and consequently need to be strong enough to resist the vertical and drag forces. However, if the overtopping flow continues for a long time, the protective layer, as well as the crest of the embankment, can fail and the underlying bed will be eroded. Besides, some of the most critical flow and geotechnical situations occur between the cover layer and the underlying soil. Characteristics of some of the protection layers, such as the filter layer, and the corresponding failures have been analyzed in previous studies (Chang and Yin, 2011; Sumer et al., 2001; Li et al., 2020; Xu et al., 2012).

In addition, to act as filters to prevent the moving of soil particles, filter layers can separate the base soil layer and the cover layer. This separation limits sediment transport and provides an appropriate surface for the protective layer. The filter layers are made of both synthetic and granular filters and reduce the hydraulic gradients behind the revetment by releasing water pressure without the loss of soil particles. Granular filters should follow a grain distribution curve to act better against scour. Smaller sizes on the base and coarser ones are to be placed on top to meet the gradual transition. A granular filter or synthetic geotextile should be placed between the subgrade and the particles (Richardson and Lagasse, 1999).

Silty sand, the combination of coarse and fine grain soil with less than 25 % of fines, has weak stability, which can increase the vulnerability of embankments (Chang and Yin, 2011). Stone dumping is one of the most popular approaches for scour protection. However, wave breaks can increase the level of turbulence, which can penetrate into the stone cover and move the sediment. Hence, the scour protection is to be designed based on the rate of turbulence and water forces are limited accordingly. One of the main design parameters which is to be considered is the ratio between the size of the sediment and that of the stones used for the protection ($\frac{d_{50}}{D}$) and Sumer et al. (2001) showed that the smaller the value of this parameter the less it is open to be removed and the penetration of the suction forces are less likely to move the particles. Multilayer stones and the installed blocks can have considerable effects on sediment transport (Nielsen et al., 2012).

Overtopping flow, which is one of the contributing factors in soil erosion, can occur during or after flooding where there is not adequate freeboard resulting in levee breach and subsequently the failure of the protective layer as it makes the soil exposed to the water and erosion happens afterwards. Another armoring technology for scour protection

is High Performance Turf Reinforcement Mats (HPTRM) in which a three-dimensional matrix of nylon filament with increased tenacity polyester reinforcement capabilities is used to mitigate soil erosion. This system lets the soil keep the moisture. Yet, it takes years for the roots to be developed (Li et al., 2020). The levee protection systems are used to protect the levees from fast-flowing and turbulent water. Slope stability of an earthen levee which was supported by High Performance Turf Reinforcement mat (HPTRM) to protect against overtopping erosion under storm surge overflow and wave and surge over-topping was studied by (Xu et al., 2012). Provided that wave force was not considerable when the surge depth increased, the factor of safety decreased. Levees' potential to stand the forces increased when strengthened by HPTRM.

2.3.1 Geotextile

As the soil loss results in failure of the structure, geotextile is considered as an environmentally friendly measure, provided that it is perfectly installed, helps stabilize the embankment. The recommended grain type/size used beneath the geotextile, permeability and role of the layer have been discussed in previous studies (Pilarczyk, 2000; Lauchlan, 1999; Escarameia, 1998). Geotextile, which is one form of Geosynthetic material, makes a flexible layer, keeping the particles beneath the filter while letting the water flow through the blocks (Pilarczyk, 2000). Geotextiles are permeable textiles or meshes which include woven and non-woven textiles. Non-woven textiles can be made for various ranges of opening sizes (Escarameia, 1998). Geo refers to the earth and second terms refer to human-made products which could be a polymer, fiberglass, among others. Geotextile is made from artificial fibers and is used to: separate the layers of the setup; act as a filter, retain some particles and let some other pass through, and reinforce by stabilizing the soil layers. Non-woven geotextile can solve this problem to some extent by placing them below the protective layer. By doing so the tiny particles are captured below the fabric. Lauchlan (1999) studied the failure mechanisms of ripraps around a cylindrical pier and found that by placing a layer of non-woven geotextile beneath the protective layer, tiny particles are captured below the fabric and the amount of sediment transport was minimized.

The important merit in using geotextiles is that they are porous to water flow through their thickness. Faure et al. (2010) studied two types of non-woven needle-punched geotextiles, a thin double layer including uninterrupted filaments and a thick layer with non-woven material. Drag force decreased with thicker geotextile covering the slope resulting in reduced soil erosion. Some of the benefits of using this material have been

mentioned herein:

- Separation

- Filteration

- Drainage

The subgrade should be sufficiently compacted and free of organic materials such as roots (Nadeau and Wedin, 2018). The geotextile is to be placed so that upstream strips overlap downstream strips (ASTM D6684).

Rock riprap is another and one of the most widely used types of scour protection used at embankments, streambeds, and bridge piers. It can significantly save sediments against scour. The higher the weight of the stones, the higher the resistance of the stones against high velocities. There are also some riprap characteristics that affect their stability such as the thickness of the stone, stone density ρ_s, location of their usage, length of the protective layer, and the grain distribution size which all have been analyzed in previous studies (Melville et al., 2006b; Mehboudi et al., 2010; Wörman, 1989; Hiller et al., 2019; Parker et al., 1998).

Packing density which is defined as the number of stones per unit area, can show the quality of the riprap placement (Hiller et al., 2019). Melville et al. (2006b) studied three different locations of scouring that occurs in the main and flood channel with the increase of the width of the flood plain from 0.8 to 2, length of the abutment from 0.4 to 1, and the width of the apron from 0 to 0.5 for riprap. Regarding the location of the scour hole the results showed, larger abutments are followed by deeper holes, and the expanded width of the apron results in making the scour hole away from the end of the abutment. As the width of the flood channel increases, the flow area at the bridge decreases, and flow velocity becomes higher and resulting in a deeper scour hole. When the scour hole is larger than the flood channel the scour depth increases.

Mehboudi et al. (2010) conducted a study on the required length of the riprap to decrease the scouring depth right after a sluice gate with the supercritical flow. They found that as the length of the riprap increases, which could break down the jet force, the depth of the scouring would decrease. If the length is less than 50 mm, the riprap cannot resist the flow and washes down in the scour hole and as the Froude number decreases (the velocity of the flow decreases), increasing the length of the riprap would be more effective. After increasing the length of the riprap beyond 50 mm, the depth of the scour hole does not change significantly. The increased weight of riprap can also help the embankment to be more resistant to higher velocities and turbulences of water flow (Melville et al., 2006b).

Wörman (1989) conducted some experiments on bridge piers protection with riprap and without any filter layer. Horseshoe and wake vortices around the pier caused increased shear stress which results in a higher rate of scour. Scouring occurs due to higher velocity and increased height of the protective layer ends up lowering the velocity of the flow and the depth of erosion would be decreased. The maximum depth of erosion

progressed within two hours in an unprotected condition. They also indicated that the movement of the bedding particles through the protection layer is affected by the parameters U^2/gS and d_{85}/D_{15}. D is the riprap median size, U is the flow velocity, and d is the base grain size. As d_{85}/D_{15} increases, the frequency of collisions between the transported particles and walls of the pores becomes larger and the filter would suffice and no transport of bed material occurs afterward. Two general riprap types usually exist, dumped and placed. Placing the stones one by one in an interlocking pattern is placed and putting the stones on the slope with random orientation can be defined as dumped riprap. In a study of the comparability of the stability of the riprap on the steep slope in both field and laboratory experiments, both placed and dumped riprap were exposed to overtopping flow and the discharge was increased to maximum capacity until failure happened and placed riprap showed more resistance, nearly 10 times higher discharge with higher critical stone-related Froude number, compared with dumped ones, however, its implementation is more expensive and takes longer (Hiller et al., 2019). Increasing the thickness of riprap layers reduces the ability to pass bedforms to undercut the layer and cause edge failure. Larger stone sizes and a thicker layer of riprap can improve the strength of the protection mechanism (Parker et al., 1998).

2.4.1 Riprap limitations

Riprap is not always accessible, particularly with the size ranges needed to protect against scour and other approaches are to be considered. It is also expensive and maybe visually unattractive. Stones should not be thin or too long. The optimal form is recommended by Federal Highway Administration to have length to Width less than or equal to 3 and the shape of the ripraps is better to be granular because of the more increased interlocking strength. The density of the particles is defined as the density of the rocks to the density of the water. The recommended equation of the ripraps weight and size based on the Federal Highway Administration is:

W = 0.85 * $(\gamma_s * d^3)$

2.4.2 riprap failures

Almost all protective layers can fail when they are exposed to a higher flow rate, than the design discharge, or placed on a poor subgrade. In terms of riprap breakdown, there are some leading factors that may affect the failure. Particle erosion, translational slide, slump, and modified slump are different forms of riprap failure (Blodgett and McConaughy, 1986; Sumer et al., 2001). The movement of the ripraps in the main
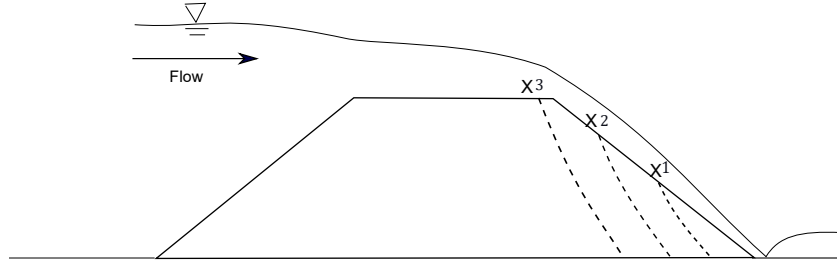
Figure 2.1: Erosion pattern with overtopping flow

channel is considered particle erosion. Increased velocity in the toe of the embankment can cause this kind of erosion to happen. Another reason is the slide of the embankment which causes the movement of the riprap if the slope is too steep. High hydrostatic pressure which reduces the frictional resistance at the interface as well as the shear along the surface can also initiate the movement. High precipitation amounts and sudden variations of water level in streams may increase the pore water pressure and result in earlier failure of riprap (Blodgett and McConaughy, 1986).

Riprap failure may happen due to Slump failure which is kind of a localized displacement of base materials that are affected by high pore pressure which decreases friction (i.e. resistance). The steep side slope is another reason for slump failure in which gravitational force surpasses the inertia forces of the ripraps. There are failure mechanisms associated with pier such as shear failure which happens when the particles cannot resist the flow horseshoe vortex resulting in pier scouring. Other mechanisms include the winnowing failure, during which, finer particles move through voids in the riprap layer and edge failure in which the edge of the coarse riprap layer starts a scour hole and initiates moving to the center of the protective layer and weaken the layer. Winnowing can further exacerbate the riprap failure.

As the overtopping flow creates higher flow velocity and shear stress. It creates a strong erosion force. When the overtopping flow is submerged, the downstream side starts to be eroded. Figure 2.1 shows the erosion pattern when overtopping flow causes the scour on the downward side of an embankment. When sediment particles are covered by armors (e.g. stones protection layer), the turbulence caused by wave force makes the subgrade particles agitated causing displacement. Sediment size, wave height, wave period, the ratio between sediment size, and protection layer can play a key role in this displacement. The turbulent water force can reach the gaps of the armor and make the sediments particles winnow out and if a considerable amount of sand is removed failure would happen. The Shields diagram has been widely used to determine the incipient motion of sediment, the critical condition in which the sediment starts to move. As long

as the Shields parameter is less than a critical value, there would be no sediment transport. Seven types of stones with sizes ranging from D= 0.65 to 10 cm were considered in this study. As d/D decreases, a higher shields value is required for sediment suction (Nielsen et al., 2012).

Sumer et al. (2001) studied the suction of the sediments below a layer of riprap. The vortices in the holes between the armor stones showed to be the main issue for the suction and removal of sediment from between stones. The sediment is circulated into the body of the flow by these vortices and is being sucked out from the holes. The Shields parameters based on the sediment size and a ratio of sediment size over the stone size(d/D) are the main reasons for this suction. d is the median diameter of the sediments and D is the median diameter of the protective layer. The results showed that the shape of the stone is not a significant factor. In general, inspection is highly crucial in ripraps, voids are to be minimized and the thickness is to be monitored. Ripraps are to be well-graded, and the maximum particle size should not be greater than twice the median size.

2.5 Articulated Concrete Blocks(ACBs)

2.5.1 Overview

An Articulated Concrete Block system (ACB) (as shown in Figure 2.3) is an alternative to riprap and other above-mentioned protection layers, which consists of an interconnected matrix of concrete block units (hard-armor products) placed across the channel. They have been used for pier scour protection, bank revetment, culvert inlet/outlet protection, pond lining, pipeline protection, dam overflow/intakes, etc. Articulated concrete block systems like other protection layers have been used to provide erosion protection to underlying soil from the hydraulic forces of moving water. These blocks can come cabled or non-cabled, open cell and closed cell. The cables in between the blocks provide a safe mat-to-mat connection and smaller mats are placed side by side and clamped together to provide a homogeneous protection system (Figure 2.2). The cables are to increase the strength and stability of the protective layer. Further, they are more flexible and more resistant than individual blocks against localized failure. The cables in between the blocks allow the individual block to be flexible and form the terrain of the ground. Stability of interlocked and individual blocks as well as pull-out tests conducted against wave attacks with different heights and interlocked blocks showed more strength against failure and needed more force to be pulled out (Gier et al., 2012). The Articulated Concrete Blocks come in four different thicknesses and heights to satisfy various required stability against water flow forces in many projects with different conditions. As an example, based on the ACBs brochure and specifications, the CC40A model mat and its cables characteristics have been shown in Tables 2.1 and 2.2.

Table 2.1: CC40A Specifications

CC40A Specifications		
System	Minimum block weight(kg/sm)	Minimum block height(mm)
CC40A	185.55-205.05	95-108

The concrete mat is being lifted with a mobile crane and carefully placed on a layer of fabric (Geotextile, etc.) to provide a smooth surface. Many studies such as (Gier et al., 2012) showed a considerable increase in stability of revetment against wave attack due to the interlocking system compared to individual blocks. The cables intercept the blocks from independently sinking down into the bed material.
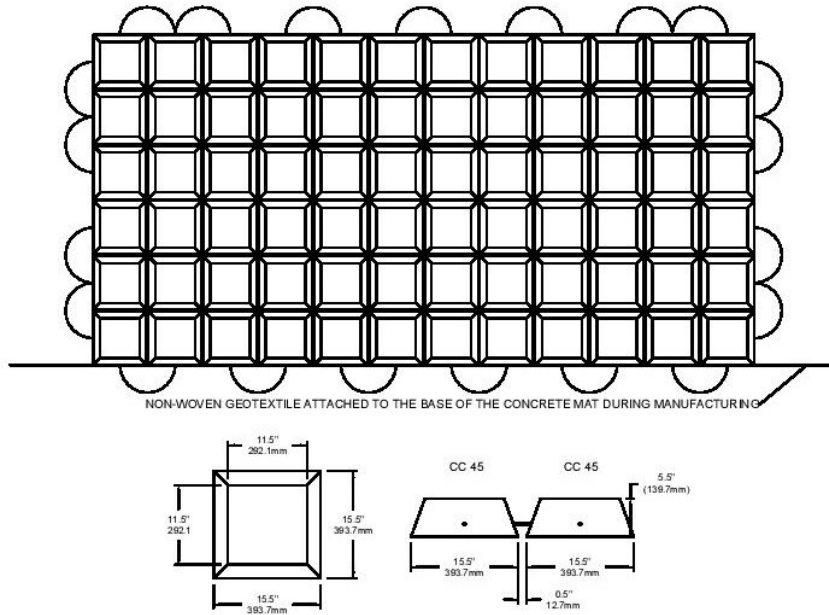
Figure 2.2: Standard CC45 Details (Credit: IECS Inc)

Table 2.2: CC40A Cables specifications

CC40A Cables specifications

System	Revetment Cable	Lengthwise(mm)	Widthwise(mm)
CC40A	Stainless Steel	4	4

Figure 2.3: An example of ACB protection (Credit: IECS Inc)

The surface beneath the protective layer is to be completely clean with no roots, debris, and stones. The Standard and Specifications (i.e, ASTM C31, ASTM C33, ASTM D698, etc.) are to be considered in both concrete batching plants and in the field for concrete, fabrics, cables, and curing.

Advantages of ACBs:

- The ability to resist flow velocities (in some conditions over 7.6 m/s) after the installation.

- ACBs are easy to install and they considerably lower the project prices.

- The topsoil can be backfilled and it is proper for vegetation growing due to the large percentage of open area within the systems.

- Can be placed underwater.

- Easier to be anchored.

- Resistant to ice damage.

- The ACB protection layer provides uniform pressure on the fabric and subgrade, which contributes to its effectiveness.

- Access to safe pedestrian and vehicles crossing can be provided because of the capability of the pressure distribution of the ACBs system.

- The system can easily be replaced and restored for future projects.

- There is up to 20-40 % open area to provide water permeability and vegetation growth.

2.5.2   Research Literature Review

The ACB includes a filter that allows infiltration and exfiltration to happen while holding onto subgrade. The effect of wave attack on the ACBs (Yamini et al., 2017), their applications on both channelized and overtopping (Abt et al., 2001), opened and closed-cell forms of the blocks (Cox,et al., 2014), the influence of block sizes and shapes and their effectiveness in scouring control (Melville et al., 2006a; Bertoldi et al., 1996) have been studied in previous research. The granular and synthetic permeable layer could possibly be used to provide sub-block pressure relief in turbulent flows or wave attack circumstances (Cox, 2010).

The stability of the protective layer depends on the flow or wave forces and the slope of embankments. Yamini et al. (2017) conducted experimental tests on the ACB under the wave attack and the effects of scaling on viscosity, surface tension, friction for four kinds of revetment with different lengths of ACB, different slopes, with and without toe and crest compartment were tested. All the experiments were conducted with scaled blocks interconnected with polyester cable in a laboratory flume. Granular and geotextile filters were considered in their study. Results showed that a mattress with a longer length has more resistance against tension forces which are distributed along the mattress length. The coefficient of mat friction (maximum slope values) on granular and geotextile was determined 36 and 29 degrees respectively after five tests for each group. Revetment

thickness and angle were changed for each type and the tensile force caused by the wave on the revetment caused a slide towards downstream. These deformations and sliding were observed for each test as the sliding was one of the key parts of the failures of the mattress after impacting the waves. Change in thickness and mass of the revetments did not affect the stability of the setup (defined based on the resistance and driving forces). The study came up with two items in stability under the impact of geotextile filter: One is the lower friction coefficient of the geotextile filter compared to the granular filter, and another one is the permeability of the construction. Although the slopes and wave effect were analyzed on the ACB, the impact of bedding with different configurations on the ACB was not considered.

ACBs can be used in different forms and on constructions with various states. Abt et al. (2001) conducted some experiments on ACBs in both channelized and overtopping flow. The overtopping flow experiments were conducted on 5H:1V and 7H:1V embankments with silty sand soil with 49 percent finer than sieve number 200. Channelized tests were done in a half trapezoidal channel with a bottom width of 1.2 ft and 2H:1V side slopes. The conditions for the tests were similar to the prototype and the blocks were placed on a concrete surface. ACBs were tested for four hours until the system failed. A non-woven geotextile was placed on top of the soil and attached to the side walls to intercept erosion down the walls. For each test depth and velocities were measured in different parts of the channel. If the test had been remained unchanged it was tested with increased flow. The maximum velocities occurred in the bottom or toe of the channel. Both overtopping and channelized tests yielded identical flow velocities and shear stress at the point of block instability. The overtopping tests showed to be more sufficient and less expensive than channelized ones. The effect of the bedding was not addressed in their experiments.

Articulated Concrete Blocks can also be used with different fabrics to better stabilize the sublayer. Following the same study, Li et al. (2014) analyzed the movement of the blocks in a large wave flume at full scale. Blocks were laid on geogrid, gravel, and geotextile on a compacted lean clay. Geotextile was to separate 10 cm gravel from 45 cm compacted clay and geogrid was used to separate gravel from the articulated concrete blocks. One piezometer, two soil strainmeters, eight soil moisture sensors, and one pressure cell were used to monitor the changes in pore water pressure, strain, total pressure, and soil moisture, respectively. The pore water pressure increased as the water was filled in the wave flume due to the seepage of water in the clay layer. There was also no considerable change of strain in the clay layer. Movement of the blocks was also considered during the tests after 6 hours of mixed surge overflow and wave overtopping.

On the crest, there was not any vertical movement in the mattress, and during the supercritical flow, the downstream movement increased. Despite the effectiveness of the geotextile beneath the ACBs, it can cause excessive force on the blocks at some points. When geotextile is used beneath the ACBs and the gravel layer is not permeable the uplift force would deform the blocks. If the geotextile works like a geomembrane the uplift force surpasses the weight of water as well as the blocks over the geotextile and the ACBs would be displaced. The hydraulic gradients $\frac{num}{den}$ can cause seepage and erosion at the exit point (Nadeau and Wedin, 2018).

The spaces between the blocks are to be optimized when placed under water flow, otherwise, it works as a low permeable protection layer. Pilarczyk (2000) studied the permeability of the mattress placed on a subgrade of clay and silty sand. They found that if the permeability of the mattress is lower than the permeability of the subsoil, the water under the mattress cannot be discharged and causes excessive lifting force on the protection layer. This will result in an increased lifting force on the mattress during wave attacks and water forces. In addition to the optimal spaces between the blocks, there should be enough space between the ACBs and any other structure as any transition can end up destabilizing the ACBs (Schweiger et al.).

The size of the blocks can affect the stability of the system. Melville et al. (2006a) tested the stability of three different block (cabled and non-cabled) sizes exposed to uniform flow. If the leading edge of the block mat was lifted the test was stopped and considered as a failed one. The different block sizes also showed different results. Block mats without cable ties failed at lower flow rates compared with the tied ones. The results showed that larger blocks need higher forces to move the block. Both cable tied concrete functions better than the individual block because it gets support from its neighboring blocks.

Articulated Concrete Blocks can be produced in various shapes, hexagonal, trapezoidal, etc. Bertoldi et al. (1996) focused on identifying the threshold of the movement for the hexagonal and trapezoidal ACBs around a rectangular pier. The blocks were put through a constant approaching flow and then the velocity was incrementally increased until the blocks failed or deformed. Hexagonal cable-tied blocks showed more strength than trapezoidal blocks because stream-lining between the hexagonal blocks is more effective than that of trapezoidal blocks. They also found that anchoring the ACBs mat to the river bed plays a significant role in its stability. Filter fabric is another crucial item in these kinds of scour protection experiments. Without filter fabric, the erosive currents induced by the pier will penetrate between each individual block and eventually cause scour.

Robeson, Thornton et al. (2005) conducted experimental tests on both opened cell and closed cell revetment ACB systems for identifying the proper threshold of failure with increasing embankment crest elevation. The water penetration was blocked in this study by using extra geotextile fabric. The facility used in their research was 4 ft wide by 110 ft long with a 2H:1V slope and 5ft overtopping depth with the toe of the embankment anchored. The configuration included two compacted layers of six-inch silty sand with the plasticity Index of three percent and the compaction content of 90 to 95 percent of standard proctor density. The ACBs were expected to survive a continuous four-hour uniform flow without any twisting and malformation. The procedure was repeated considering higher discharge rates at each interval. Hourly measurements of water depth and velocity were collected at 2 to 4 intervals for water surface elevations and point velocities respectively. The test was continued until the maximum capacity was reached or at when deformation or soil loss occurred. The length of the embankment was decided to be shortened after the failure of the closed-cell ACBs during which the blocks were deformed after 8 minutes and the highest lift was roughly 15 cm of the peak of the failure. By doing this, the test continued for four hours continuously with 1 foot overtopping. Closed-cell ACB was deformed with one-foot overtopping, whereas the open cell ACB was deformed with a three-foot depth of the overtopping flow. The bedding effect was neglected in this study and just the overtopping flow was considered.

Some of the failure mechanisms include:

- Separation of the blocks from the subgrade may result in erosion, settlement, or liquefaction of the embankment soil.

- Loss of contact with the embankment soil may happen by moderate erosion down the slope, which can result in sediment transport through joints.

- Uplift of the center, overturning, and rolling up of the leading edge particularly when they are not sufficiently anchored.

The sand beneath the ACBs block is to be non-erodible, otherwise, the overtopping flow could wash out the sand and cause deformation under the layer. Voigt et al. (1998) studied the failure and incipient motion of the blocks on an embankment consisting of highly erodible soil in a study at Minnesota University, silty clay soil with low plasticity was compacted to 90 percent based on the compaction proctor test and then the two different sizes of ACBs were installed on a non-woven geotextile. The tests were conducted for an embankment with a 2:1 slope. 1 foot overtopping and the discharge of 24 cfs was considered and after the completion of the run, the misplacements of the blocks were

measured. This test was followed by 2-foot overtopping with the discharge of 78 cfs for four hours and 3-foot with a discharge of 152 cfs and 3.5 feet with the discharge of 198 cfs. As the side slope condition was not addressed in this study, minimized allowable velocity and shear stress were recommended when ACBs are laid on the side slopes of an embankment.

Parker et al. (1998) studied the effect of the thickness of the block mat on their failure. The ACBs were tested for hydrodynamic stability and performance characteristics and the highest shear stress, as well as highest velocity, were obtained 38.5 lb/ft^2 and $19.0 ft/s$, respectively. Increasing block thickness and unit weight showed increased stability for the tests.

Scour shapes can be different when blocks are used as the protective layer around constructions or abutments. Regarding the variations of scour shapes by modifying the abutment geometries and the toe required protection Melville et al. (2006b) conducted a study to compare the functionality of Cable tied blocks and riprap. Variations of the length, as well as the width of the abutment over the flow depth in the considered flood channel, were modified and longer abutments ended up with larger scour holes. The minimum required width for the scouring protection increases by increasing the length of the abutment over-flow depth in the flood channel. As the width of the flood channel increases the area at the bridge section decreases and consequently the velocity increases and a deeper scour hole happens afterward. Scour holes for Cable Tide Blocks (CTBs) tests formed closer to the abutment compared to that of riprap protection. The protection layer did not reduce the depth of the local scour but changed the distance of the scour from the abutment.

There are some leading elements that could be regulated to minimize the probability of the ACBs failure. Both shear stress and velocity at stability threshold are used for designing criteria for ACBs revetment system. Regarding the loss of a block, if there is an adequate force to initiate overturning, the system is considered to have reached the stability threshold if the base of any block has lost touch with the filter (ASTM 7277). One of the influential factors in the failure of the cable concrete is the safety factor which is not be addressed in this study. Regarding the stabilized stone drainage layer on the performance of the blocks, there is also a threshold when the block is uplifted from contact with the filter. Considerable siltation which does not stabilize over time shows uplift of the revetment system. Should one or two blocks lose their connection with the subgrade, the stability threshold was met. This threshold could help the hydraulic design parameters be determined with an appropriate factor of safety (Nadeau and Wedin, 2018).

In many of the studies conducted so far:

- The bedding was neglected and only the overtopping effect of the water flow was analyzed on the blocks

- The experiments were conducted on similar subgrade and configurations

In this study, this gap has been addressed and the objectives are as follows:

- Stability of the bedding and indirect failure of the ACBs due to the overtopping flow is considered

- Different soil materials with different characteristics and grain sizes with various configurations, different thicknesses of the layers, and two different slopes are analyzed.

- The influential parameters that affect the erosion are identified along the channel segments

- Optimal subgrade configurations for the ACB for both 14 and 26.6-degree slopes are recognized

Bibliography

S. R. Abt, J. R. Leech, C. I. Thornton, and C. M. Lipscomb. Articulated concrete block stability testing 1. *JAWRA Journal of the American Water Resources Association*, 37 (1):27–34, 2001.

S. Amaral, T. Alvarez, L. Caldeira, T. Viseu, and R. Ferreira. Recent advances on experimental dam breach studies.

C. Auel, I. Albayrak, and R. M. Boes. Bedload particle velocity in supercritical open channel flows. In *River Flow*, pages 923–9331, 2014.

C. Auel, I. Albayrak, T. Sumi, and R. M. Boes. Sediment transport in high-speed flows over a fixed bed: 2. particle impacts and abrasion prediction. *Earth Surface Processes and Landforms*, 42(9):1384–1396, 2017. URL https://onlinelibrary.wiley.com/doi/full/10.1002/esp.4132.

D. Bertoldi, J. Jones, S. Stein, R. Kilgore, and A. Atayee. An experimental study of scour protection alternatives at bridge piers. 1996.

J. Blodgett and C. E. McConaughy. *Rock riprap design for protection of stream channels near highway structures: Volume 2–Evaluation of riprap design procedures*, volume 2. US Geological Survey, 1986.

C. S. Chang and Z.-Y. Yin. Micromechanical modeling for behavior of silty sand with influence of fine content. *International Journal of Solids and Structures*, 48(19):2655–2667, 2011.

A. L. Cox. *Moment stability analysis method for determining safety factors for articulated concrete blocks*. PhD thesis, Colorado State University, 2010.

B. Dargahi. Controlling mechanism of local scouring. *Journal of Hydraulic Engineering*, 116(10):1197–1214, 1990.

B. Dargahi. Scour development downstream of a spillway. *Journal of hydraulic research*, 41(4):417–426, 2003.

F. Delgado-Ramos, J. M. Poyatos, and F. Osorio. Internal erosion of clayey soils protected by granular filters. *La Houille Blanche*, (4–5):42–47, 2012.

M. Escarameia. River and channel revetments. *Des. Man*, 20:245, 1998.

Y.-H. Faure, C. C. Ho, R.-H. Chen, M. Le Lay, and J. Blaza. A wave flume experiment for studying erosion mechanism of revetments using geotextiles. *Geotextiles and Geomembranes*, 28(4):360–373, 2010.

F. Gier, H. Schüttrumpf, J. Mönnich, J. Van Der Meer, M. Kudella, and H. Rubin. Stability of interlocked pattern placed block revetments. In *Proceedings of the Coastal Engineering Conference (2012)*. Reston: American Society of Civil Engineers, 2012.

P. H. Hiller, L. Lia, and J. Aberle. Field and model tests of riprap on steep slopes exposed to overtopping. *Journal of Applied Water Engineering and Research*, 7(2): 103–117, 2019. doi: 10.1080/23249676.2018.1449675. URL https://doi.org/10.1080/23249676.2018.1449675.

R. Joustra. Interface stability in granular open filters in unidirectional flows: investigating the required minimum filter layer thickness for stable geometrical open filters in unidirectional flows. Master's thesis, University of Twente, 2013.

T. Kenney and D. Lau. Internal stability of granular filters. *Canadian geotechnical journal*, 22(2):215–225, 1985.

P. F. Lagasse. *Countermeasures to protect bridge piers from scour*, volume 593. Transportation Research Board, 2007.

C. S. Lauchlan. *Pier scour countermeasures*. PhD thesis, ResearchSpace@ Auckland, 1999.

L. Li, F. Amini, Y. Pan, and C. Li. Stability monitoring of articulated concrete block strengthened levee in combined wave and surge overtopping conditions. In *Geo-Congress 2014: Geo-characterization and Modeling for Sustainability*, pages 262–271, 2014.

L. Li, F. Amini, Y. Pan, S. Yuan, and B. Cetin. *Hydraulics of Levee Overtopping*. CRC Press, 2020.

A. Mehboudi, J. Attari, M. Saneie, and M. M Tabatabai. Effect of bed protection length on local scour downstream of horizontal jets. *Journal of Hydraulics*, 5(1):37–49, 2010.

B. Melville, R. Van Ballegooy, and S. Van Ballegooy. Flow-induced failure of cable-tied blocks. *Journal of Hydraulic Engineering*, 132(3):324–327, 2006a.

B. Melville, S. Van Ballegooy, S. Coleman, and B. Barkdoll. Countermeasure toe protection at spill-through abutments. *Journal of Hydraulic Engineering*, 132(3):235–245, 2006b.

N. C. Nadal and S. A. Hughes. Shear stress estimates for combined wave and surge overtopping at earthen levees. Technical report, ENGINEER RESEARCH AND DEVELOPMENT CENTER VICKSBURG MS COASTAL AND HYDRAULICS LAB, 2009.

J. Nadeau and B. Wedin. The effect of a stabilized stone drainage layer on acb performance in open channel flow applications. 2018.

A. W. Nielsen, B. M. Sumer, and J. Fredsøe. Suction removal of sediment from between armor blocks. iii: Breaking waves. *Journal of Hydraulic Engineering*, 138(9):803–811, 2012.

G. Parker, C. Toro-Escobar, and R. L. Voigt Jr. Countermeasures to protect bridge piers from scour. 1998.

M. M. PASHA, A. H. MAHMOOD, and S. SHAMS. An analysis of scouring effects on various shaped bridge piers.

K. Pilarczyk. *Geosynthetics and geosystems in hydraulic and coastal engineering.* CRC Press, 2000.

M. Rasaei, S. Nazari, and S. Eslamian. Experimental and numerical investigation the effect of pier position on local scouring around bridge pier at a 90° convergent bend. *Journal of Hydraulic Structures*, 6(1):55–76, 2020.

E. V. Richardson and P. F. Lagasse. *Stream stability and scour at highway bridges.* ASCE Publications, 1999.

P. Schweiger, D. Shaffer, and J. Nadeau. *ACB armoring potential failure modes at dam embankments and spillways.* PhD thesis, Colorado State University. Libraries.

B. M. Sumer, S. Cokgor, and J. Fredsøe. Suction removal of sediment from between armor blocks. *Journal of hydraulic engineering*, 127(4):293–306, 2001.

A. Wörman. Riprap protection without filter layers. *Journal of Hydraulic engineering*, 115(12):1615–1630, 1989.

Y. Xu, L. Li, and F. Amini. Slope stability analysis of earthen levee strengthened by high performance turf reinforcement mat under hurricane overtopping flow conditions. *Geotechnical and Geological Engineering*, 30(4):893–905, 2012.

O. A. Yamini, M. Kavianpour, and S. H. Mousavi. Experimental investigation of parameters affecting the stability of articulated concrete block mattress under wave attack. *Applied Ocean Research*, 64:184–202, 2017.

S. A. Zomorodian and M. J. Moghadam. Investigation of effective parameters on the embankment dam filter behavior in simultaneous cracking in the core and filter. *Geotechnical and Geological Engineering*, 29(4):637–644, 2011.

Chapter 3

Methodology

3.1 THEORETICAL APPROACH

3.1.1 Flow Pattern

As the experiments were conducted on an embankment (using a broad crested weir structure), the flow pattern followed the gradually varied flow equations and the direct step method was used to calculate the hydraulic variables.

3.1.2 Gradually varied flow (GVF)

Gradually varied flow follows the two fundamental hydraulics equations: energy and continuity.

$$E_w = \frac{U^2}{2g} + y + h_0 \tag{3.1}$$

The energy equation with respect to the flow direction along the channel is as follows:

$$\frac{dE_w}{dx} = \frac{d(U^2/2g)}{dx} + \frac{dy}{dx} + \frac{dh_0}{dx} \tag{3.2}$$

The LHS defines the rate of change in energy on the downward direction.

$$Fr = \frac{V_c}{\sqrt{gY_c}} = 1 \tag{3.3}$$

$$\frac{dy}{dx} = \frac{S_0 - S_f}{1 - F^2} \tag{3.4}$$

F = Froude number $F = v/(gh)^{0.5}$ where v defines the flow velocity, g is the gravitational acceleration, and h is the height of the water flow.

In overtopping flow, the flow starts from the crest, accelerates along the slope to the downstream until the flow is developed. when Fr < 1, the flow is subcritical; when Fr > 1, the flow is supercritical; when Fr = 1, the flow is critical. In this study, the Froude number is always more than one as the flow is supercritical on the downward slope.

The open channel flow is characterized based on the Froude number, which represents the relationship between gravity and inertial forces. In an open channel or natural stream, the effect of a grade or slope tends to increase the flow velocity along the flow path. Gravity is opposed by frictional resistance, which increases with velocity, and eventually, the two are balanced in a uniform flow condition. When the two forces are not in balance, the flow is nonuniform and is called gradually varied flow if changing conditions occur over a long distance and exist in a steady but nonuniform flow. Gradually varied flow occurs when there is an abrupt change or transition confined to a short distance. In this study, a sudden change in slope from sub-critical to critical and supercritical on the downstream happens. The condition of critical flow just defined is used to define channel slope. If for a given roughness and shape, the channel slope is such that the uniform flow is subcritical, the slope is said to be mild and y > yc. If the uniform flow is supercritical, the slope is termed steep and y < yc which happens in our research it starts from Yc to the normal depth which is S2. A critical slope Sc is a slope that will just sustain a given rate of discharge in a uniform flow at critical depth. The lower arm in Figure 3.1 shows the supercritical velocity. In this study, steady flow existed as the discharge remained stable and it was non-uniform flow as the velocity and depth varied along the embankment.

For the rectangular channels, the critical depth can be derived by taking the derivative of the energy equation and setting it to zero. The energy associated with the critical depth is found by placing the critical depth expression into the specific energy equation. The E-y curve is the variation of Energy to y for a given value of q in an open channel.

$$Y_c = (\frac{q^2}{2g})^{1/3} \tag{3.5}$$

$$E_{min} = (\frac{3}{2})Y_c \tag{3.6}$$

3.1.3   Broad Crested Weir

The broad crested weirs are hydraulic structures widely used for depth control and flow measurement in fields and laboratories. Two broad crested wooden structures (with different downstream slopes) were used in this study to setup the embankment (and

29
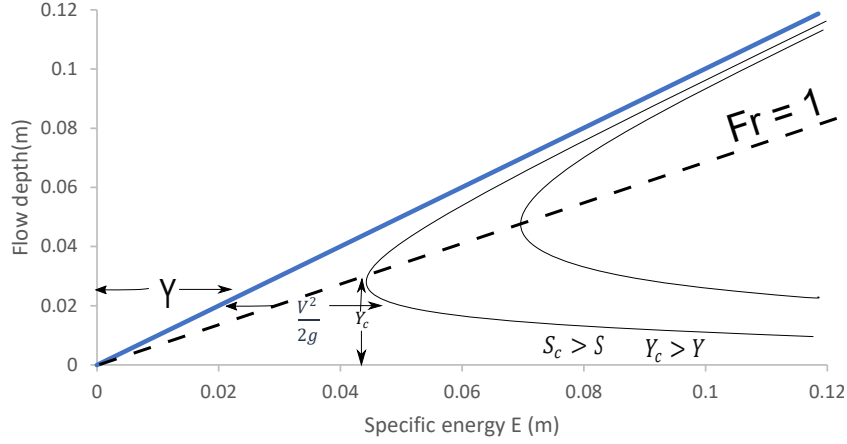
Figure 3.1: E-y curve

minimized the influence of seepage), and the water surface profile over the crested weir was measured in the laboratory. The steady overflow discharge per unit length over a broad crested weir in an open channel flow is as follow (Minimal frictional energy loss along the crest is assumed):

$$q_S = (\frac{2}{3})^{3/2} \sqrt{g} h_1^{3/2} \tag{3.7}$$

For critical flow $F_R = 1$

$$q_c = \sqrt{g h_c^3} \tag{3.8}$$

$$h_c = \frac{2}{3} h_1 \tag{3.9}$$

v_c is the critical overflow velocity

$$v_c = \sqrt{g h_c} \tag{3.10}$$

g is gravity acceleration
h_1 is upstream head

The flow on the landward side of the embankment follows the Chezy and Manning equations:

$$v_0 = (\frac{\sqrt{sin\theta}}{n})^{3/5} q_0^{2/5} \tag{3.11}$$

$\theta =$ landward side slope angle
$q_0 =$ steady critical discharge m^2/s

30
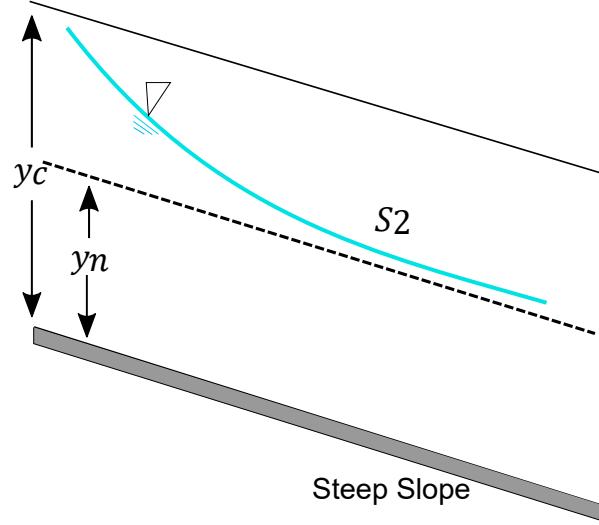
Figure 3.2: Water Surface profile

n = Manning's roughness

$$\tau_0 = \rho g \frac{(h_1 + h_2)}{2} sin\theta \tag{3.12}$$

$$u_* = (\frac{\gamma S R}{\rho})^{1/2} \tag{3.13}$$

Chezy equation and Shear velocity:

$$V = c\sqrt{gsR}, \quad V = cu_*, \quad \frac{V}{u_*} \tag{3.14}$$

$$Y_2 + Z_2 + \alpha_2(\frac{V_2^2}{2g}) = Y_1 + Z_1 + \alpha_1(\frac{V_1^2}{2g}) + h_e \tag{3.15}$$

Water flow velocity, discharge, shear stress, and other variables can be calculated along the channel using Manning's and Chezy equations.

3.1.4 Direct Step Method

Figure 3.3 shows the water surface profile in this study which is classified as Gradually Varied Flow profile. The curves are based on the hydraulic slope which is steep $(S_0 > S_c)$ and the flow is supercritical$(y_c > y_n)$.

The water surface profile is to be traced along the channel to calculate the variables. The Energy Equation for open channel flow is used, which includes pressure head, elevation head, and velocity head. Atmospheric pressure was negligible in this study. The
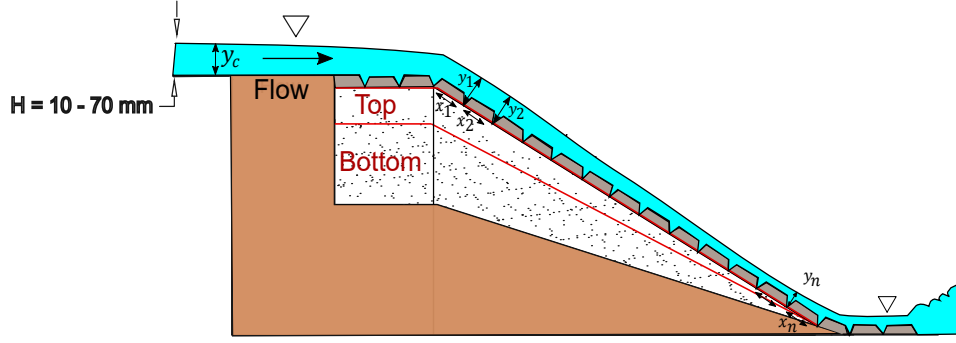
Figure 3.3: Direct step method (the water flow starts from critical depth on the crest and reaches the normal depth on the downstream)

reach was divided into several segments with $\delta y = 0.001$ m per step to get accurate results, and specific energy was calculated and compared at two points. Computations were to proceed from the upstream. On the upstream side of the embankment, the flow condition was critical, in which the mean specific energy was minimum. y_c was measured on the upstream perpendicular to the bed of the embankment. The discharge per unit width was calculated based on the Broad crested weir formula and was verified with the Flowmeter in the hydraulics flume (Chanson, 2004).

Broad Crested Weir Discharge:

$$q_S = (\frac{2}{3})^{3/2} \sqrt{g} h_1^{3/2} \tag{3.16}$$

Law of conservation of Energy

$$P_2 - P_1 = (mgh_2 - mgh_1) + [\frac{1}{2}mV_2^2 - \frac{1}{2}mV_1^2] \tag{3.17}$$

Bernoulli Equation:

$$\frac{V^2}{2} + gz + \frac{p}{\rho} = constant \tag{3.18}$$

V = fluid flow speed
g = acceleration due to gravity
z = elevation of the datum
p = pressure point
ρ = density of the fluid flow

$$S_0\, dl + y_1 + \frac{V_1^2}{2g} = y_2 + \frac{V_2^2}{2g} + S_f\, dl \tag{3.19}$$

32

$$(S_0 - S_f)\,dl = (y_2 + \frac{V_2^2}{2g}) - (y_1 + \frac{V_1^2}{2g}) = E_2 - E_1 \tag{3.20}$$

$$\bar{S}_f = \frac{S_{f1} + S_{f2}}{2} \tag{3.21}$$

$$dl = \frac{\delta E}{S_0 - \bar{S}_f} \tag{3.22}$$

For the channel bottom slope steeper than 1:10 (5.71 degrees, $\cos(\theta) = 0.995$) the vertical pressure head (incremental y along the channel as shown in Figure 3.3) was not considered as d and was multiplied by cos ($\theta = 26.6$ and 14 degrees) to avoid the very small error in estimating the vertical depth.

A Python function was developed to implement the direct step method. This function uses the SymPy library to solve the equations using the inputs provided by the user. The inputs are the width of the channel (b), Manning's (n), slope (s), acceleration due to gravity (g), and water depth (h), as shown in Appendix A. The function calculates the area, perimeter, radius, velocity, energy equation, SE(), ΔX, and Froude number using the value of water depth in different segments (y) calculated from Energy and Manning's Equations. The user can provide multiple values for Manning's, slopes, and water depth; and the function writes all the calculated values in a separate excel file for each set of inputs (See Python Function).

3.1.5   Sediment

The rate of erosion depends on the type of the soil, compaction water content, grade of saturation, the velocity of the water flow, the slope of the embankment, etc. Finer grained soils erode quickly and have lower resisting shear stress compared with coarser-grained soils. Well-vegetated overbanks, riprap channels, and Articulated Concrete Blocks can control the scouring caused by the surface flow (Lee and Hedgecock, 2008). Hence, identifying these variables help realize the potential amount of sediment transport and local erosion along the channel.

Critical velocity can be defined as follows:

$$V_c = K_u \times Y^{1/6} \times D^{1/3} \tag{3.23}$$

V_c= minimum critical velocity that material with size D and smaller will be moved in (ft/s)

$K_u = 11.17$

y = average depth of flow upstream from the contraction(ft)

Shear velocity and shear stress are the most important factors in designing all the protection layers and assessing their deformation and instabilities. Design velocity is not to exceed the critical shear stress. Regarding the flow around a bend, velocity can range between 0.9 and 1.7 times the cross-section mean velocity (NCMA, 2010).

3.1.6   Bedding

Failure of the Articulated Concrete Blocks relates to its bedding and sublayer. When the bedding or the layer below the protection layer erodes, failure happens. Shear failure happens when the force on the particle exceeds the resistance force (when the force is large enough to wash the soil the erosion happens subsequently), winnowing, and edge failure occurs. As the bedding in this study is movable, recognizing the sediment transport and sediment movement condition is crucial. Regarding the movement of the finer particles sucked out from between the coarser particles (Sumer et al., 2001) recorded the motion of a single particle trapped in a hole and identified the following forces:
Some of the driving forces that cause the particle to be sucked out include drag and pressure-gradient force and resistance force which is mostly due to the submerged weight of the finer particles preventing this action to happen.

Needless to say that higher driving force makes the particle more prone to be sucked out. And larger particles need the larger value of Shields parameter to move the particle. They also came to realize that if the holes between armors become deeper than a certain value the driving force cannot make the trapped particle move. Sediment transport conditions are regime, threshold, and rigid. Regime channel beds are the ones that are moving in most of the flow conditions and mostly they are sand or silt size noncohesive materials. Threshold channel beds have no motion at lower flows but they initiate moving at higher flows and this threshold is to be defined in each scenario. Rigid beds are based on boulder size and hardly ever start to move. This study is of mobile bed models as the sediment transport was considerable and Shields parameter of the bed material $\tau_* > 0.06$ (Julien, 2010). The bedding beneath the geotextile in this study was movable. Critical shear stress and shear velocity based on the Shields parameter help identify the initiation of motion of sediment.
The shear velocity which is a kinematic substitute for the dynamic bed shear stress τ_0 is as follows:

$$U_* = \sqrt{\frac{\tau_0}{\rho}} = \sqrt{gR_hS_f} \tag{3.24}$$

U_* = shear velocity

τ_0 = shear stress

R_h = hydraulic radius

ρ = water density

g = gravitational acceleration fluid and friction velocity is provided by Chezy coefficient c_z:

$$c_z = \frac{U}{U_*} \tag{3.25}$$

and the bed roughness is known as roughness Reynolds number Re:

$$Re = \frac{U_*D}{\nu} \tag{3.26}$$

$$\tau_c* = \frac{\tau_c}{(\gamma_s - \gamma)d} \tag{3.27}$$

$$\tau* = \frac{\tau_0}{(G - 1)gd} \tag{3.28}$$

τ_c is the critical shear stress for incipient motion which is dependent on particle characteristics such as volumetric mass (ρ_s) and particle size (d_m). τ_* is related to the water depth and slope.

When the load over the bed exceeds the critical value the particle starts to move

$$\tau = \gamma_w \, y \, S_e \tag{3.29}$$

τ = shear stress due to fluid force

γ_w = unit weight of water

y = depth of flow

S_e = energy slope

Particles are to be large enough to stand the shear forces and small enough to intercept the erosion of the bedding particles. Shear stress which is derived from the conservation of momentum is the force applied by the flowing water of its boundary. The boundaries in the study were the blocks and channel surface. For uniform flow the energy slope is as follows:

$$S_e = \frac{v^2 n^2}{y^{4/3}} \tag{3.30}$$

S_e = energy slope

v = velocity

n = Manning's

For a particle to be displaced, the dimensionless bed shear stress or the Shields stress is to be higher than τ_c^*. Shields diagram shows a relationship between dimensionless critical stress and the shear Reynolds number. Brownlie (1981) provided a formula based on Shields data.

$$\tau_c^* = 0.22 \times R_{ep}^{-0.6} + 0.06exp(-17.77R_{ep}^{-0.6}) \tag{3.31}$$

3.1.7 Dimensional Analysis

Dimensional analysis was done to determine the numerical value and the units of the variables in an equation. The relationships between various physical quantities can be derived from dimensional analysis. By doing so, the effect of the leading variables can be recognized. To make the equations dimensionally homogeneous, the dimensional analysis of the parameters shows the nondimensional relation for the parameters. pi theorem presents a physical law that gives a relation between the physical variables (Curtis et al., 1982). In this theory, an equation can be rewritten based on a certain number of physical relevant variables (n) and independent dimensions (m). Hence, a relationship between (k = n - m) and non-dimensional parameters Π_1, ..., Π_{n-m} is made. Then based on the repeating variables, the non-dimensional parameters Π are constructed. The setup in this study possesses 10 degrees of freedom because all the variables could be changed for each setup.

$$\delta = f(Q, \mu, \rho, V, D_{50}, \rho_S - \rho, U*, g, t, H, S, \theta_c) \tag{3.32}$$

k = n - m = 11 - 3 = 8 number of Πs

For instance, the first Π is shown below:

$$\Pi_1 = \delta V^{a1} D_{50}^{b_1} \rho^{c_1} : \Pi_1 = \{(L^3)(\frac{L}{T})^{a_1}(L)^{b_1}(\frac{M}{L^3})^{c_1}\} \tag{3.33}$$

By equating the powers, the new equation is derived.

$$M : 0 = c_1; L : 0 = 3 + a_1 + b_1 - 3c_1; T : 0 = -a_1 \tag{3.34}$$

36

$$\frac{\delta}{D_{50}^3} = f\left(\frac{Q}{D_{50}^2 V}, \frac{t}{D_{50}}, \frac{\mu}{D_{50} V \rho}, \frac{g D_{50}}{V^2}, \frac{U^*}{V}, \frac{H}{D_{50}}, \frac{\rho_S - \rho}{\rho}, S, \theta_c\right) \tag{3.35}$$

δ = soil loss after each test(L^3); the rate of mass removal per unit area

Q = discharge $\left(\frac{L^3}{T}\right)$

v = velocity $\left(\frac{L}{T}\right)$

g = gravitational acceleration $\left(\frac{L}{T^2}\right)$

ρ = density $\left(\frac{M}{L^3}\right)$

μ = viscosity $\left(\frac{M}{LT}\right)$

t = thickness of the layers (L)

ρ_s = sediment density $\left(\frac{M}{L^3}\right)$

D_{50} = particle size (L)

U^* = shear velocity $\left(\frac{L}{T}\right)$

H = water depth (L)

s = slope of the embankment

θ_c = critical shear stress

The experimental tests were conducted using a hydraulics flume to assess the indirect failure mechanisms of the Articulated Concrete Blocks based on the standard installation procedures (based on the prototype conditions) and identify the optimal subgrade configuration. Nine experiments were performed with different soil types but without the protection layer. Afterwards, 31 tests were carried out with the cable concrete and various configurations on two wooden broad crested weir structures considering bed slopes of 14 and 26.6 degrees. Figure 3.5 shows the 14-degree embankment in the hydraulics flume.

3.2.1   Flume

The experiments were conducted in a 5m-long, 31cm-wide flume with a height of 47cm and maximum discharge of 0.014 m^3/s in the hydraulics lab of the Civil and Environmental Engineering department at Western University (Figure 3.5). Figure 3.4 shows the schematic of the flume in the hydraulic lab.
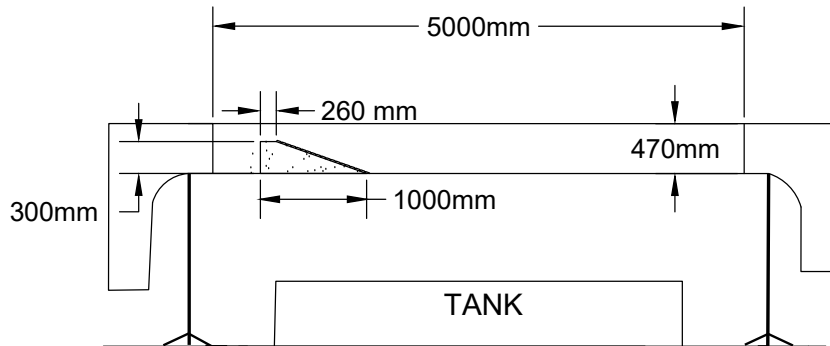
Figure 3.4: Flume schematic

3.2.2   Embankment

A wooden block with a steep gradient was used to characterize the overtopping flow conditions by reducing the effects of seepage (Figure 3.7). The model tests in the flume were investigated following the prototype conditions. Profile view of the ACB, subgrade and the wooden structure is shown in Figure 3.6. The crest height of the model setup is 300 mm from the bottom of the flume and the length of the crest is 260mm. The length of the downstream slope is 1250 and 520 mm for 14-degree and 26.6-degree slope tests, respectively. The broad crested weir was made out of wood for the tests and the

Figure 3.5: Hydraulics Flume at Western University

horizontal crest is to be adequately long to carry on the hydrostatic pressure distribution and maintain the supercritical flow on the landward-side slope.
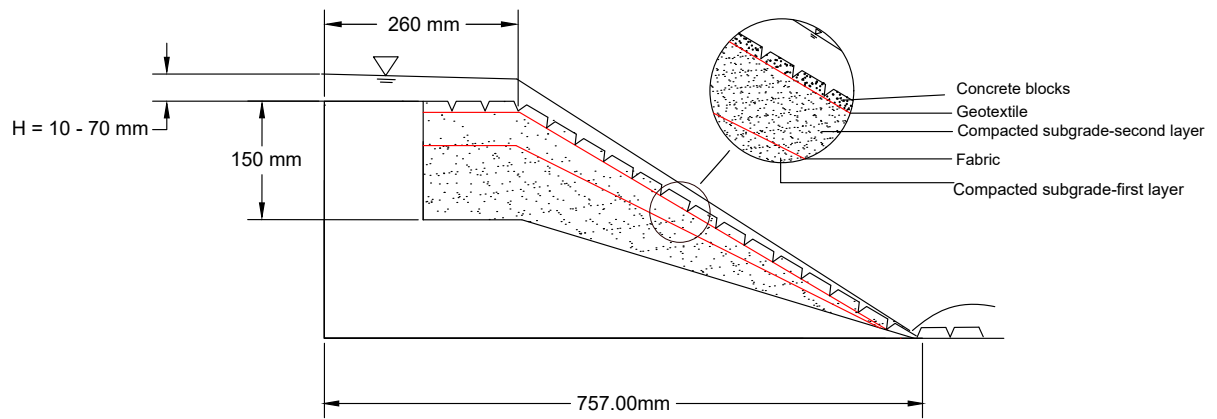
Figure 3.6: Setup for the scaled model test (26.6-degree slope) and the overtopping flow is from the left to the right

Figure 3.7: Wooden structure

3.2.3 Scaled Blocks

Articulated concrete blocks have non-woven needle-punched geotextile installed prior to the installation when used in the prototype (Figure 3.8). However, the blocks and filter fabrics may or may not be used along with the ACBs. In this study, the stability of scaled Articulated Concrete Blocks was analyzed considering various overtopping flow conditions based on industry approved design procedures. All the products were tested according to the concrete standards and specifications (Figure 3.9 (a)).

The scaled interlocked blocks consist of rows of metal ropes, each row is laterally offset by two-half of a block width and interconnected with four other blocks (Figure 3.9 (b)). In the prototype, the geotextile fabrics were pre-attached to the blocks but in the tests, fabrics were not attached to the blocks to be changed and modified for each different tests configurations. Non-woven geotextile which is one of the geosynthetic types was used in this study to provide a barrier between the soil layers, when dissimilar soil was used, and prepare a smooth surface for the block mattress. It also serves as a filter underneath the protection layer. Geogrid is also a separator and works as a drainage system. For clarity of presentation, the physical characteristics of the ACB products and materials are provided in Table 3.1.

ACBs are made with ordinary Portland cement type I compliant with requirements of ASTM C150 along with normal river sand and gravel. After mixing the ingredients, the concrete is cast in molds and covered with a plastic layer to prevent evaporation for 24

Figure 3.8: Blocks with geotextile attached (Credit: IECS Inc)

Table 3.1: Physical Characteristics of Individual ACB Mat Systems

Width (cm)	Length (cm)	Thickness (cm)
4.8	4.8	2.7

<center>(a)   (b)</center>

Figure 3.9: (a) Concrete samples based on standards and specifications; (b) Scaled Blocks (Credit: IECS Inc)

h. Afterward, the ACBs were demolded and cured under laboratory conditions at 20 ± 3 degrees centigrade and 100% humidity. The fresh properties of the concrete. including slump and density, is tested according to Standards and specifications. Furthermore, the compressive strength of 150x300 mm cylindrical samples cured for 28 days is measured. Accordingly, the concrete had a slump and density of 100 mm and 2300 kg/m3, respectively. The 28-day compressive strength is measured as 30 MPa.

3.2.4 Experimental variables and materials

Variation in subgrade configuration plays a key role in stabilizing or weakening the ACB setup. Multiple factors can affect scouring including flow rate and depth, the slope of the embankment, sediment size, density, and the thickness of the layers. In this study, we assessed the influence of these factors based on a suite of experiments. The variables are shown in Table 3.2.

<center>Table 3.2: Experimental variables</center>

Water depth on the crest (mm)	Embankment slope (degree)	Thickness of the layers	Fabrics	Soil types
10 to 70	14 and 26.6	1-2 and 1-5	Geotextile, Geogrid, and more permeable filter cloth	Soil with $D_{50}=$ 0.55 to 12 mm

3.2.5 Soil

Different soil types and particle sizes show different erosion resistance behavior. Tests with various configurations and materials were conducted to evaluate the corresponding effectiveness to control scouring and soil loss. Figure 3.10 shows the different soil types used in the experiments.
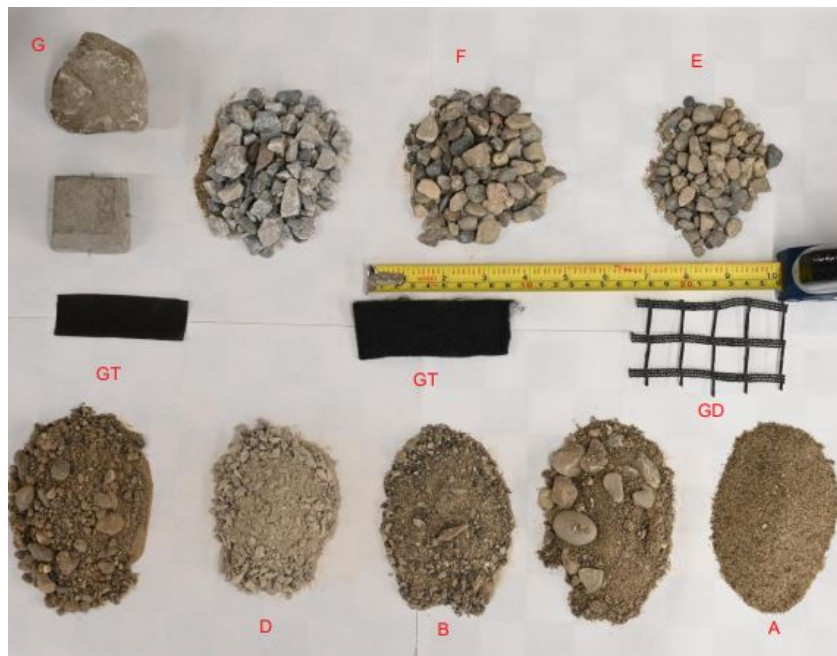
Figure 3.10: Different soil types and fabrics used in the experiments

Geotechnical Tests

Geotechnical tests (sieve analysis, compaction proctor test, direct shear, hydraulic conductivity, porosity, soil moisture content(%)) were conducted for each soil sample.

(a)   (b)   (c)

(d)

Figure 3.11: (a) Sieve analysis; (b) Compaction proctor test; (c) Hydraulic conductivity; (d) Direct shear

Soil Characteristics

Sieve analysis was conducted for all the samples based on (ASTM, 2006) as shown in Figure 3.12.
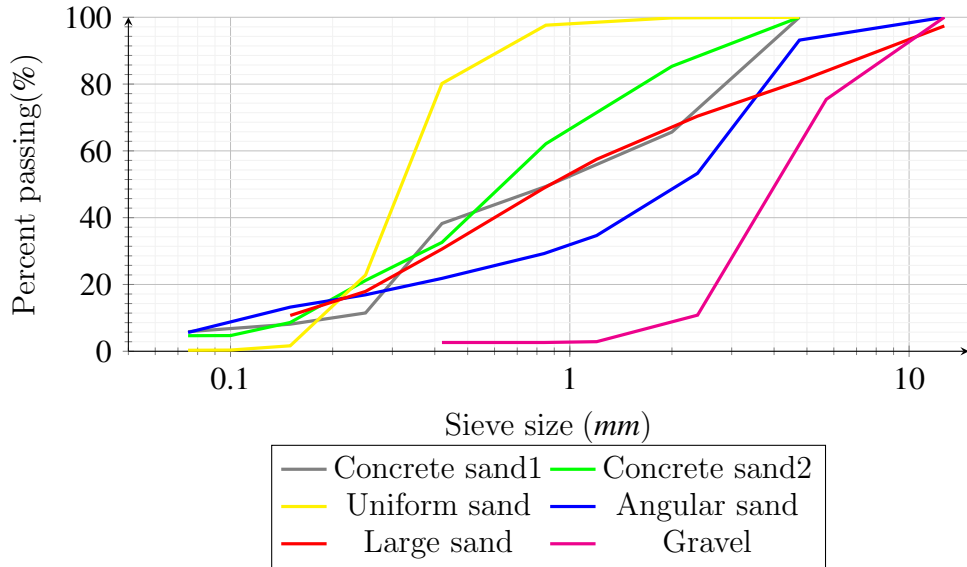
Figure 3.12: Sieve analysis

Tables 3.3 and 3.4 illustrate the results for all the soil samples based on the Unified Soil Classification Systems and laboratory tests.

Compaction Proctor Test

The strength of dry soil increases as water is added to it (w_{opt}). The optimum amount of water enables soil particles to better slide to each other. On the other hand, an excess amount of water can decrease the stability of the soil. The standard proctor compaction curve based on the dry unit (γ_d) and water content(w) was considered for the compaction of soil layers and are presented in Figures 3.13. These figures illustrate the maximum density and the optimum moisture for two of the soil types. Soils were compacted with an optimum moisture content between 85 to 95 percent of the standard proctor test based on (Brand, 2015).

Table 3.3: Soil characteristics

Soil types	Median diameter (D_{50})	Uniformity coefficient (C_u)	Coefficient of curvature(C_c)	Hazen Eq	Hydraulic conductivity	Geometry standard deviation
Concrete sand1	0.65	10	0.71	0.04	0.06	4.2
Concrete sand2	0.60	5.33	1.33	0.04	0.05	3.6
Uniform sand	0.55	1.5	1.1	0.05	0.07	1.5
Angular sand	2.1	12	0.9	0.012	0.015	3.7
Large sand	0.90	10	0.75	0.03	0.05	4.4
Gravel	3.5	2.2	1.2	4.9	7.2	1.8

Table 3.4: Properties of sediment

Properties of sediment

Sediment particles characteristics	Equations	Range
Specific weight of solid particles, γ_s	$\gamma_s = \rho_s g$	$26.0 KN/m^3$
Specific gravity G	$G = \frac{\gamma_s}{\gamma}$	2.65
Submerged specific weight of a particle, γ_s'	$\gamma_s - \gamma$	-
Sediment size d_s	very coarse sand(>1.00 mm)	-
Geometry Standard Deviation	$\sigma_g = \sqrt{\frac{d_{84}}{d_{16}}}$	1 - 6.48
Hazen (cm/s)	$c\,D_{10}^2$	0.0000001 - 1
Cavity (n)	$n = \frac{e}{1+e}$	
Porosity (e)	$K(cm/s) = 2.4622\left(D_{10}^2\left(\frac{e^3}{1+e}\right)^{0.7825}\right)$	
Dry unit weight	$\gamma_d = \frac{\gamma}{1+\omega}$	
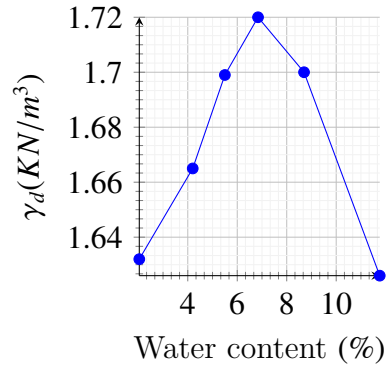
(a) D_{50}=0.55 mm
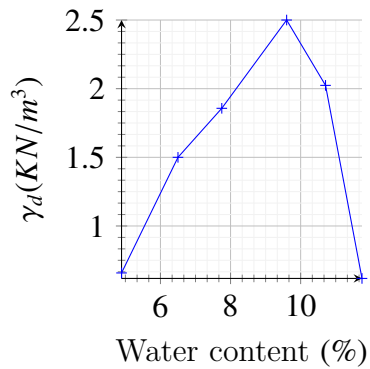
(b) D_{50}=0.65 mm

Figure 3.13: Compaction proctor test for two different soil types

Direct Shear Test

The Direct Shear test was done based on (Brand, 2008) to determine the shear strength of soil materials used in this study. The aim of this test is to determine the maximum resistance that a material can stand. The shear strength of the geotechnical materials can be described by Mohr-Coulomb's equation:

$$\tau = c + \sigma_n \tan \phi \tag{3.36}$$

τ = shear strength

c = cohesion

σ_n = normal stress

ϕ = angle of internal friction

The equation represents a straight line on shear strength versus normal stress plot (Figure 3.14). The intercept on the y-axis is the cohesion(c) which is zero for the materials used in this study. The slope of the line is the angle of internal friction(ϕ).

48
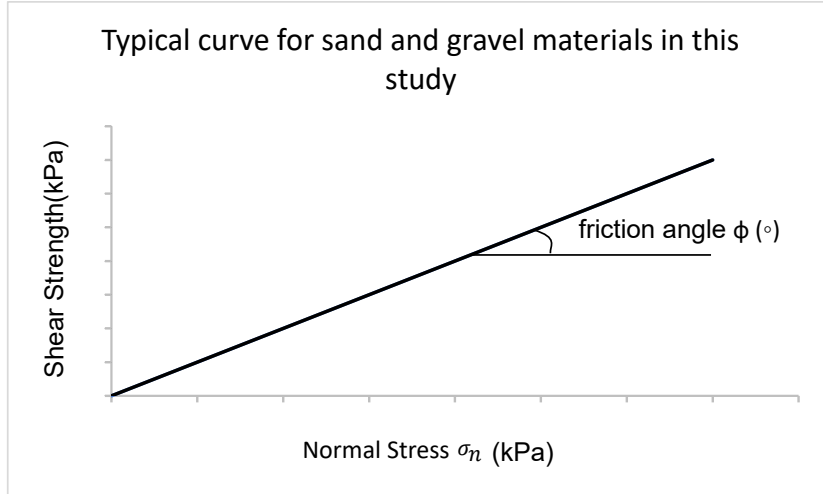
Figure 3.14: Shear strength- Normal stress curve for the materials in this study

3.2.6　Hydraulic Characteristics

In addition to the bedding characteristics, hydraulics variables were defined and analyzed, as shown in Table 3.5. The discharge rate started from 0.002 m^3/s and the maximum discharge could be 0.014 m^3/s. The flow was supercritical in these experiments. Hence, the Froude numbers initiated from 1 (corresponding to the critical depth on the crest of the embankment) and reached more than 1 on the landward side of the embankment. The flow depth on the horizontal crest started from 10 *mm* with the minimum discharge and reached 70 *mm* when the discharge was maximum.

Table 3.5: Hydraulic characteristics

Hydraulic characteristics	
Hydraulic parameters	range of variables
Discharge rate	0.002-0.014 $\frac{m^3}{s}$
Froude number	1 - 4
Flow depth	10 - 70 mm

49

3.3 EXPERIMENTAL PROCEDURE

All the experiments were conducted based on the general field installation procedure. 9 preliminary tests with five different soil types, on slopes 26.6 (2H:1V) and 14 (4H:1V) degrees, without any protection layer were implemented to analyze the stability of the native soil and observe how the embankment reacts to the water flow when the slope was not stabilized (as shown in Tables 4.1 and 4.6). Next, 31 experiments were performed to assess the stability of the ACB mat exposed to similar overtopping flows considering various subgrade configurations.

3.3.1   Different Configurations

The failure occurrence depends on various configurations and different setups. Sediments in this study were affected by multiple factors including flow rate, slope, sediment size and density, and the thickness of the layers, as discussed previously.
Different configurations in this study were based on various variables which were changed in each experiment. Variables (see 3.10) are written in abbreviation as follows:
Slopes of the structures: S = 26.6-degree slope, M = 14-degree slope.
Fabrics: GT = Geotextile, GD = Geogrid.
Thickness of the layers: 1-2: thickness of the bottom layer = 100 mm: thickness of the top layer = 50 mm
1-5: thickness of the bottom layer = 125 mm: thickness of the top layer = 25 mm Grain size diameters: Sand: A: D_{50} = 0.55 mm, B: D_{50} = 0.65 mm, C: D_{50} = 0.9 mm, D: D_{50} = 2.1 mm Gravels: E: D_{50} = 3.5 mm, F: D_{50} = 10 mm, G(riprap): D_{60} = 60 mm.
Trench 1 = A core sand filled with soil D and the same sand on the sides and downstream.
Trench 2 = A core sand filled with soil D and polymeric sand on the sides and downstream.
Trench 3 = A core sand filled with soil D and gravel E on the sides and downstream.
Figure 3.15 shows the variables and the experimental procedure for the experiments conducted in the lab. The abbreviation of some of the different possible configurations used for the experiments for both 14 and 26.6-degree slopes is shown in Table 3.6. For instance, test "M-GT-B-1-2" configuration include compacted soil with D_{50} = 2.1 mm on the bottom layer with the thickness of 100 mm, followed by a layer of geotextile, compacted soil with D_{50} = 0.65 mm on the top layer with the thickness of 50 mm, and a layer of geotextile on the top below the ACB mat. For all the experiments, geotextile was used between the bottom and the top layer, and just the fabric below the ACB mat was changed.

01 Variables and materials

01 Slopes
- S = 26.6-degree (2H:1V)
- M = 14-degree (4H:1V)

02 Thickness of the layers
Bottom: Top layer thickness ratio
- 1-2
- 1-5

03 Fabrics
- GT = Geotextile
- GD = Geogrid

04 Discharge

	Rate (m^3/s)	Water depth on the horizontal crest (mm)
Min	0.002	10
Max	0.014	70

05 Grain size diameters

Sand:
A = D_{50} = 0.55mm
B = D_{50} = 0.65mm
C = D_{50} = 0.9mm
D = D_{50} = 2.1mm

Gravel:
E = D_{50} = 3.5mm
F = D_{50} = 10mm

02 Experimental procedure

01 Compaction of the bottom layer uniformly based on the Compaction Proctor test.

02 Placing one layer of geotextile between the bottom and the top layer.

03 Compaction of the top layer to provide a uniform surface for the concrete blocks.

04 Placing one layer of geotextile on the top layer. Geotextile can be used for sand and gravel and Geogrid can be used for gravel only.

05 Putting the ACB mat from toe to the top and attaching the layer to the upstream, let the water flow (initiates from 10 mm) passes through the layer. The test run continues until the water depth reaches 70 mm and if any soil loss happens, the experiment would be stopped and the failure and amount of the soil loss would be recorded.

03 Data collection and analysis

2 GoPro and Nikon Z7
→ Collecting data before, after, and during the experiments

Kinect
→ 3D plots to calculate the amount of soil loss in each test
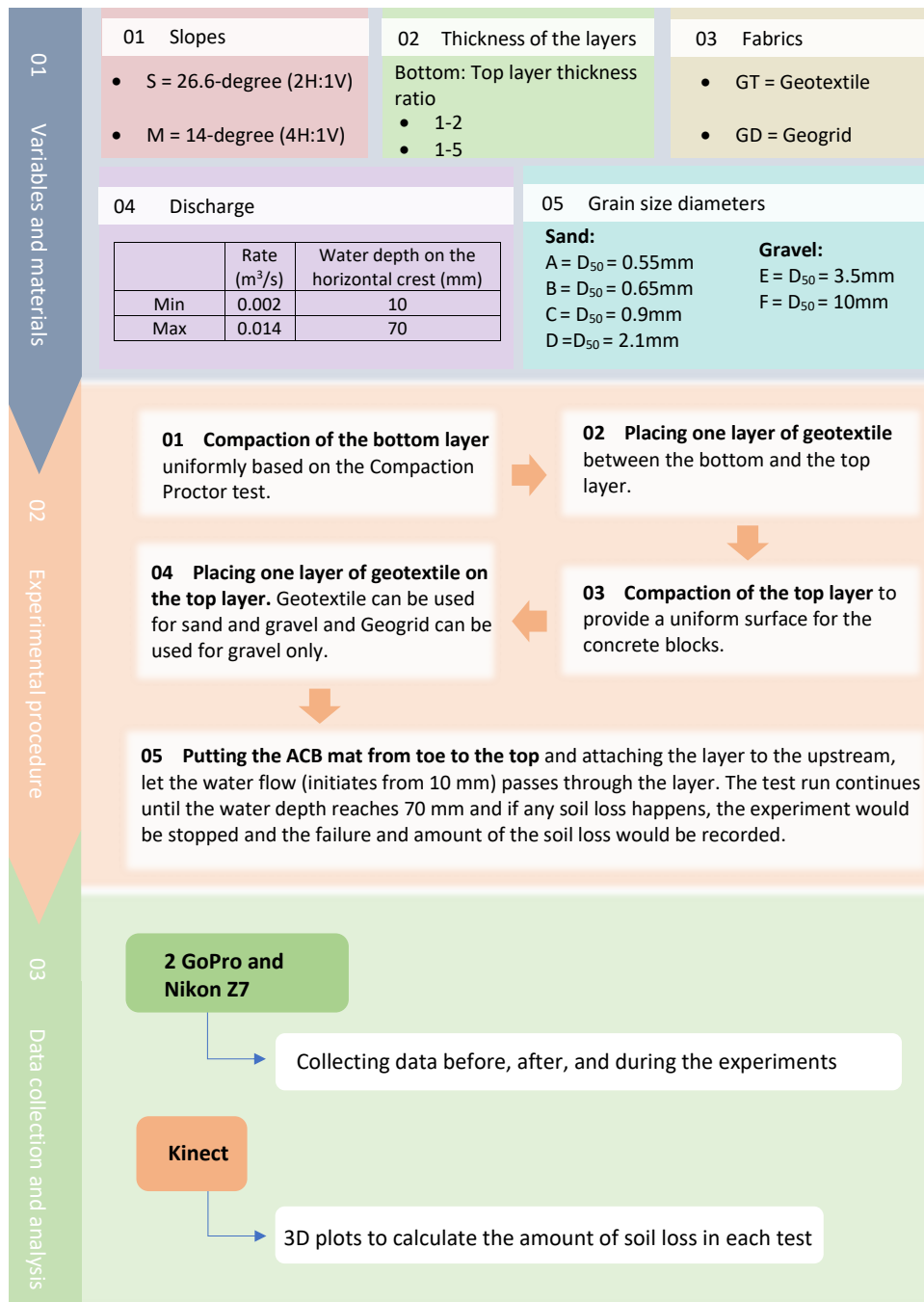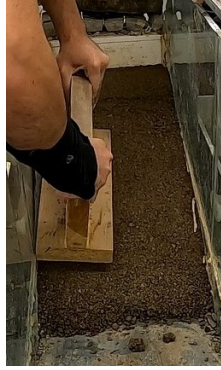
Figure 3.15: Experimental procedure

Table 3.6: Different configurations on both 14 and 26.6-degree slopes

| Experiments | Configurations | | | |
	Bottom layer D_{50} (mm)	Top layer D_{50} (mm)	Fabric	t
M-GT-B-1-2	2.1	0.65	GT	1-2
M-GT-C-1-2	2.1	0.9	GT	1-2
M-GT-D-1-2	0.65	2.1	GT	1-2
M-GD-E-1-2	2.1	3.5	GD	1-2
M-GD-E-1-5	2.1	3.5	GD	1-5
S-GT-B-1-2	0.65	0.65	GT	1-2
S-GT-C-1-2	0.9	0.9	GT	1-2
S-GT-D-1-2	2.1	2.1	GT	1-2
S-GT-E-1-2	2.1	3.5	GT	1-2
S-GD-E-1-5	2.1	3.5	GD	1-5

The subgrade was mixed with the appropriate amount of water based on the compaction proctor test outputs and was placed and compacted layer by layer (in 1-cm layers) uniformly with care between the vertical glass walls. In the next step, geotextile or filter cloth was placed on the bottom layer to separate the bottom and top layers. On the top layer, the mixture of soil and water was placed and compacted in 1-cm layers. Then, another layer of the fabric was placed on the top layer without any wrinkle and ups and downs to prepare the bedding for the protection layer. To account for the bedding effect, the fabrics were not attached to the sides to allow for water infiltration underneath the fabrics. The scaled blocks were carefully placed on the fabrics to avoid unintentional movement of the fabric as they were not pre-attached to the blocks. On the upstream side of the embankment, the blocks were attached to the wooden structure to prevent any displacement of the mat. Each test included a continuous 10-minute flow over the revetment system with constant discharge. The threshold considered in failure of each test was based on the soil loss and deformation of the blocks or loss of contact of the blocks with the subgrade. On the condition that the setup survived the 10-minute flow without exceeding the defined threshold, the procedure was repeated with higher discharge and this process repeated until the threshold was met. The maximum discharge and velocity that the system could resist were recorded and reported. Flow depth can play a key role in scouring. For each test the discharge was released with the minimum rate of 0.002 m^3/s and depth of 10 mm on the horizontal section and stepwise increased in 10-min intervals until any movement was detected, soil loss was observed and the threshold was met. The amount of soil loss was extracted using the 3D recorded images by a Kinect. A threshold was defined for the failure of the tests when any movement of the blocks, and scour happen. All the experiments were recorded with two GoPro-8 and Nikon Z7 for top view and side view respectively.

In the horizontal crest, the flow was critical and the Froude number was equal to 1. On the downstream the flow was supercritical and F > 1, assuming that the backwater effects are neglected. Prior to the preliminary tests, blocks were placed without any anchor on the slope and block weights were the only resistance force against the uplifting force. At the embankment toe, a hydraulic jump could occur and at some points, the tailwater continued to rise above the toe, which could accelerate the scour process. Figure 3.16 shows one of the experimental procedures for the construction of the embankment with a trench (Table 4.2).
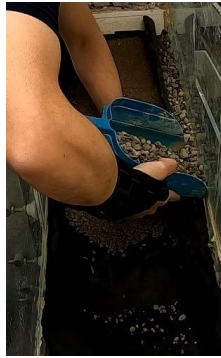
(a) Compaction of the bottom layer

(b) Geotextile

(c) Compaction of the top layer

(d) Gravel on the sides

(e) Pipe

(f) Gravel on the downstream

(g) Mattress of the blocks

(h) Maximum discharge

(i) After the test

Figure 3.16: Experiment procedure

3.3.2 Monitoring Procedure

The progress of the experiments was measured and recorded using high speed cameras (Nikon Z7 with 45.7MP BSI-CMOS sensor with native ISO 64, and GoPro 8 with 12MP sensor) from overhead and both sides, before, after the completion, and during each test for different analyses.

Kinect V2 was used in the study to create a 3D model of surfaces before and after each test to measure the amount of soil loss in each test (Figure 3.17). This motion sensor camera helps assess the changes in the morphology of the channel. Kinect simulates spatial data in three different axes (X, Y, Z). By capturing each photo, depth measurements are produced. Data are filtered in MATLAB to extract the DEM. By subtracting the two matrixes of data points (one before and one after the test is conducted), the amount of soil loss is calculated for all the experiments. By doing so morphology of the failed embankment is derived and can be compared with other configurations and setups.
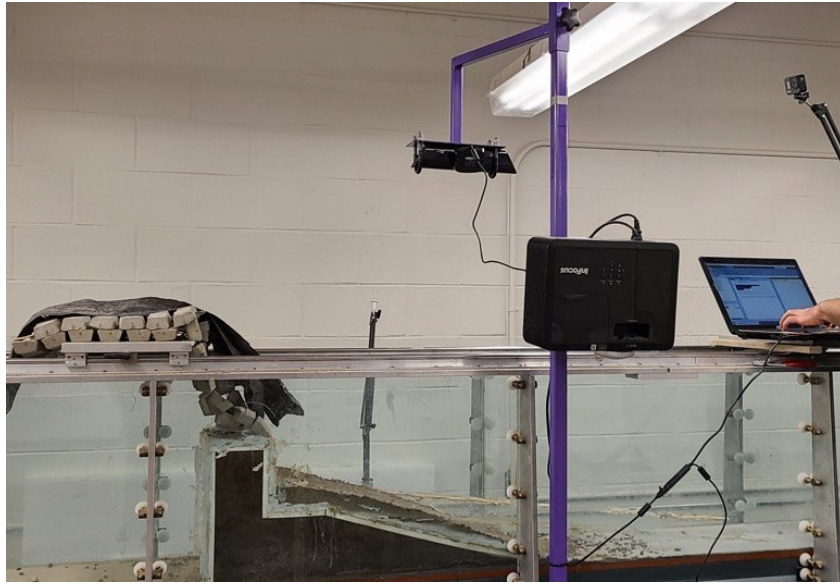

Figure 3.17: Kinect used in each experiment to provide the 3D plots to calculate the amount of soil loss in each trial

The velocity and discharge for different configurations can be shown in graph 3.18. This graph compares the velocity (derived from the direct step method) for both 14 and 26.6-degree slopes according to the same discharge and water depth on the horizontal crest. By increasing the water depth on the crest, the discharge can be derived and compared with the flowmeter underneath the flume.
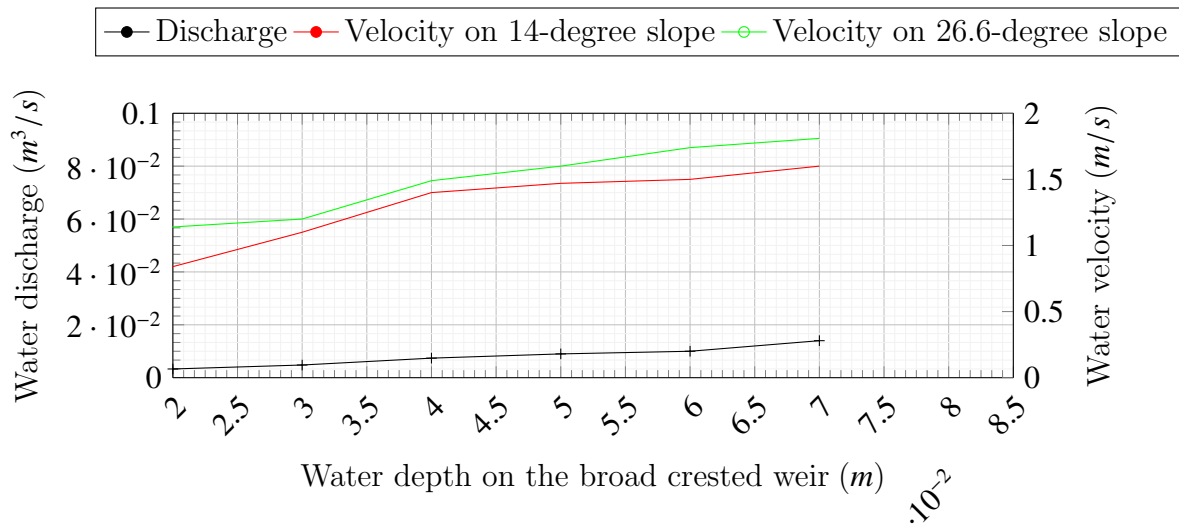

Figure 3.18: Water depth-velocity for 14 and 26.6-degree slopes

Bibliography

I. N. Aribudiman, I. W. Redana, K. D. Harmayani, and Y. Ciawi. Seepage in soil from the difference of water viscosity using geo-studio seep/w program. *Int. Research Journal of Engineering, IT & Scientific Research*, 5:15–26, 2019.

C. ASTM. Standard test method for sieve analysis of fine and coarse aggregates. *ASTM C136-06*, 2006.

L. Brand. Standard test method for performing laboratory direct shear strength tests of rock speciments under constant normal force. 2008.

L. Brand. Standard test method for laboratory compaction characteristics of soil using standard effort. pages PA 19428–2959, 2015.

W. R. Brownlie. Prediction of flow depth and sediment discharge in open channels. 1981.

H. Chanson. *Hydraulics of open channel flow*. Elsevier, 2004.

W. Curtis, J. D. Logan, and W. Parker. Dimensional analysis and the pi theorem. *Linear Algebra and its Applications*, 47:117–126, 1982.

P. Y. Julien. *Erosion and sedimentation*. Cambridge university press, 2010.

K. Lee and T. Hedgecock. Clear-water contraction scour at selected bridge sites in the black prairie belt of the coastal plain in alabama, 2006. Technical report, Geological Survey (US), 2008.

M. R. Najafi and A. R. Zarrati. Numerical simulation of air–water flow in gated tunnels. In *Proceedings of the Institution of Civil Engineers-Water Management*, volume 163, pages 289–295. Thomas Telford Ltd, 2010.

P. K. Singh, S. Banerjee, B. Naik, A. Kumar, and K. K. Khatua. Lateral distribution of depth average velocity & boundary shear stress in a gravel bed open channel flow. *ISH Journal of Hydraulic Engineering*, 27(1):23–37, 2021.

B. M. Sumer, S. Cokgor, and J. Fredsøe. Suction removal of sediment from between armor blocks. *Journal of hydraulic engineering*, 127(4):293–306, 2001.

T. Tingsanchali and C. Chinnarasri. Numerical modelling of dam failure due to flow overtopping. *Hydrological Sciences Journal*, 46(1):113–130, 2001.

S. Wang, M. R. Najafi, A. J. Cannon, and A. A. Khan. Uncertainties in riverine and coastal flood impacts under climate change. *Water*, 13(13):1774, 2021.

Chapter 4

# Results and Discussions

4.1 EXPERIMENTAL RESULTS

Failure of the setup and the embankment depends on the subgrade configuration and the water flow characteristics. Both the water flow and subgrade features were changed and analyzed in this study. Before and after each experiment photographs and DEM files were taken and recorded with measuring devices to compare the stability of the tests. Figure 4.1 shows the experiment S-GT-D-1-2 in which soil D (see Section 3.3.1) was used on the bottom and top layers on 26.6-degree slope followed by a layer of geotextile and the ACBs. Figure 4.2 illustrates the Kinect outputs for the test with the amount of soil loss calculated using MATLAB. Figure 4.3 presents the experiment S-GD-E-1-5 which was stable during the test and remained unchanged and Figure 4.4 shows the kinect outputs for this test. Figure 4.5 shows the amount of soil loss using the difference of the matrix of data points before and after each test. The amount of soil loss (δ) derived for each experiment is shown in Table 4.2.

(a)	(b)

Figure 4.1: (a) Subgrade (sand) before the test was conducted and (b) after the failure
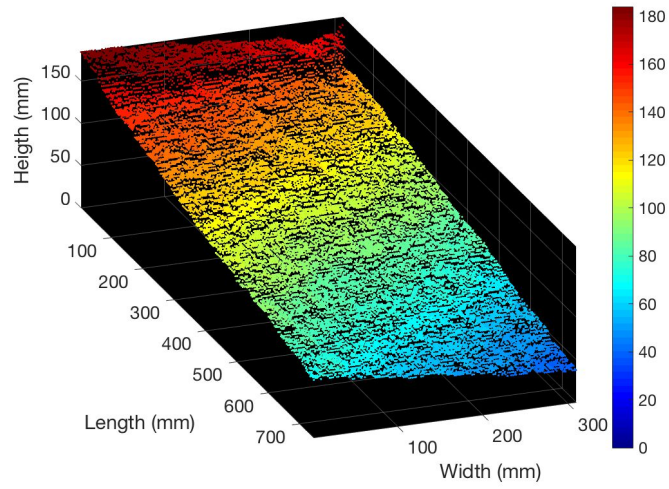
(a) Kinect output; bottom layer-before the failure
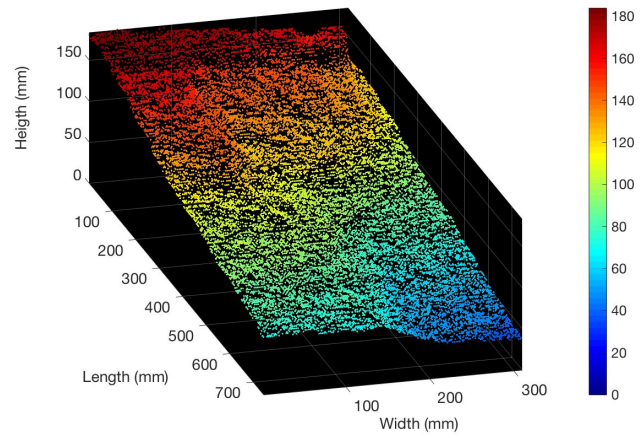
(b) Kinect output; bottom layer-after the failure

Figure 4.2: Kinect DEM outputs for the sand before the test conducted(a) and (b) after the failure

(a) Gravel-before the failure   (b) Gravel-after test was conducted

Figure 4.3: (a) Gravel with the $D_{50} = 3.5$ mm after the compaction; (b) shows that the gravel remained stable after the test was conducted and there was not any soil loss happened
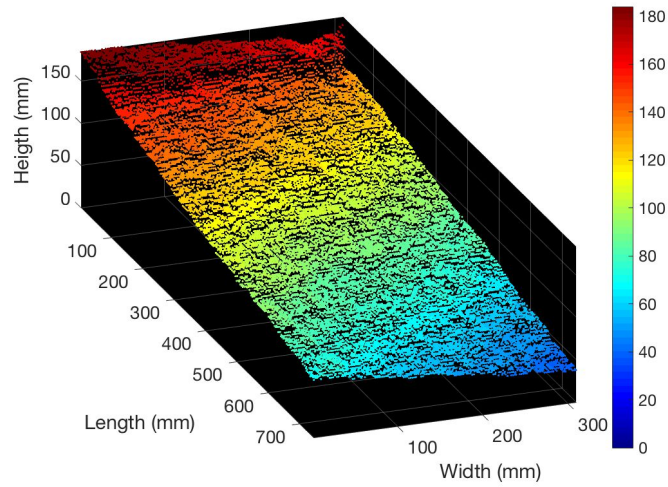
(a)
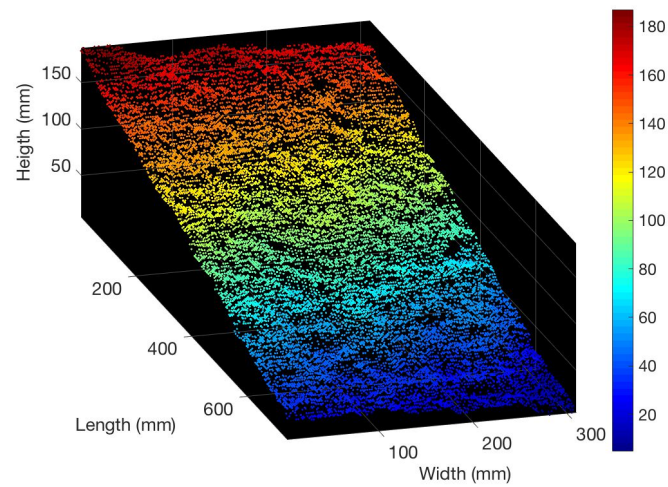
(b)

Figure 4.4: Kinect DEM outputs: (a) the gravel with the $D_{50} = 3.5$ mm after the compaction and (b) shows that the gravel remained stable after the test and there was not any soil loss happened
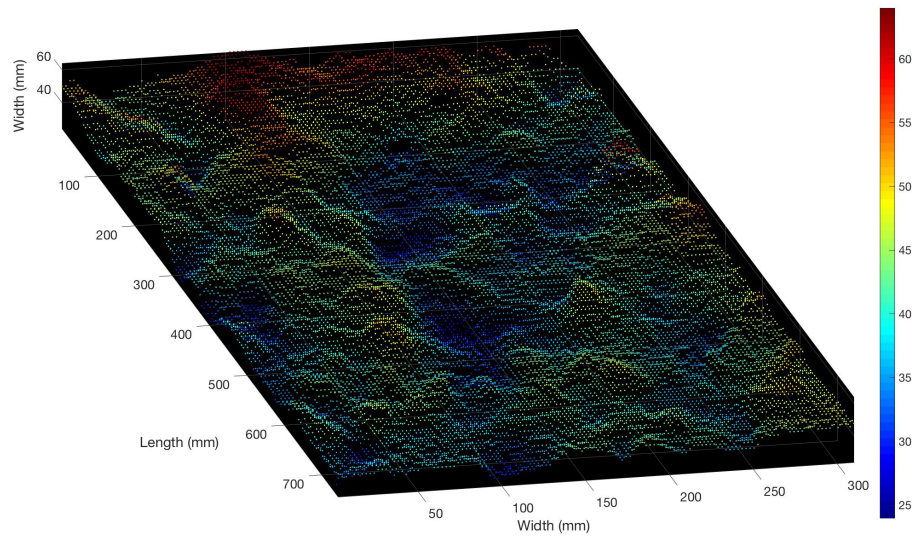
(a)
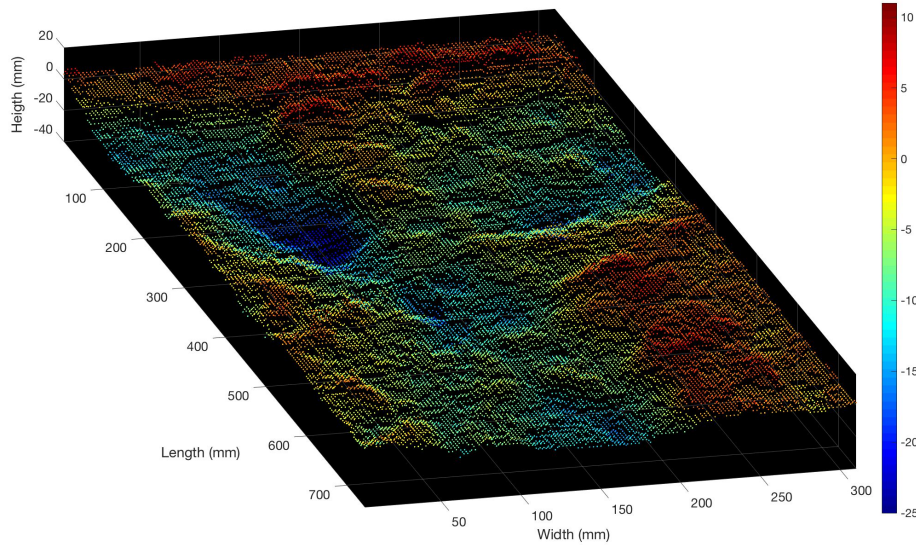
(b)

Figure 4.5: Difference in the volume of soil loss when sand and gravel used with the protective layer based on Kinect DEM outputs: (a) shows the difference of the volume of soil loss in setup with sand layer; (b) shows the difference of the volume of soil loss in setup with gravel layer
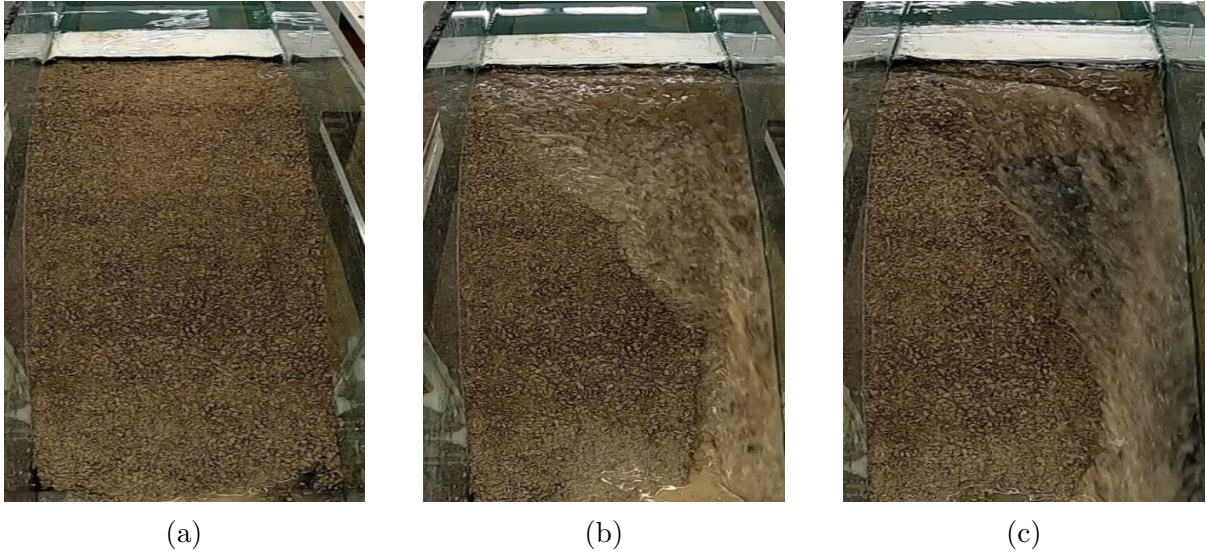
Figure 4.6: Test results corresponding to S-GT-D-1-2 in different time steps (seconds):
a) 00.00; b) 00.06; c) 00.08

Table 4.1 shows the results of the preliminary tests without the blocks for both 14 and 26.6-degree slopes. All the tests failed in less than 10 seconds. As expected, failure took longer in the 14-degree slope compared to the one in 26.6-degree slope. Figure 4.6 shows the test "S-GT-D-1-2" which was conducted without any protective layer. The embankment was washed down in less than 10 seconds.

The flow characteristics and failure mechanism of the preliminary tests on the 26.6 and 14-degree slopes are as follows:

- Velocity on the downstream 14-degree slope $= 0.65$ m/s; 26.6-degree slope $= 0.9$ m/s; riprap with $D_{50} = 60$ mm on the 26.6-degree slope $= 1.1$ m/s

- Maximum discharge resulted in failure of the set up $= 0.002$ m^3/s

- Shear stress (14-degree slope) $= 6$ N/m^2; 26.6-degree slope $= 9$ N/m^2; riprap with $D_{50} = 60$ mm on the 26.6-degree slope $= 10$ N/m^2

Table 4.1: Summary of the parameters considered in the preliminary experiments without ACBs. Q: Maximum Discharge; V: Maximum velocity; δ: Soil loss

Experiments	Q (m^3/s)	V (m/s)	δ $(\%)$
S-GT-C-1-2	0.002	0.9	100
S-GT-B-1-2	0.002	0.9	100
S-GT-D-1-2	0.002	0.9	100
S-GT-G-1-2	0.0048	1.1	100
M-GT-C-1-2	0.002	0.65	80
M-GT-D-1-2	0.002	0.65	70
M-GT-E-1-2	0.002	0.65	55

31 experiments were performed to assess the stability of the ACB mat exposed to overtopping flows considering various subgrade configurations.

The experiments were conducted on the 14-degree slope with sand (D_{50} = 0.65, 0.9, 2.1 mm) and gravel (D_{50} = 3.5, 10 mm). An experiment was conducted with a specific configuration and the following tests were repeated with different particle sizes, different fabrics, different methods of compacting the two layers of soil, and different methods of putting the fabrics to find the optimal design and for each experiment, the results of which were recorded. In terms of the time of the experiments, 10 minutes was considered as many of the failed initial tests failed in this period. However, this duration was increased for the stable embankments up to an hour for each discharge rate to make sure the system remained stable. These procedures were repeated for the 26.6-degree slope as well.

4.1.1 Tests on the embankment with a 14-degree slope

Test "M-GT-C-1-2" with fine sandy soil was conducted on 14-degree slope. The subgrade configuration corresponding to the "M-GT-C-1-2" test consists of:

1. Bottom layer: sand with D_{50} = 2.1 mm was placed and compacted (with the thickness of 100 mm) followed by a layer of geotextile.

2. Top layer: sand with D_{50} = 0.9 mm was placed and compacted (with the thickness of 50 *mm*) followed by another layer of geotextile and the ACB mat.

The flow characteristics and failure mechanism of this test are as follows:

- Velocity on the downstream = 0.91 m/s

- Maximum discharge resulted in failure of the setup = 0.0065 m^3/s

- Shear stress = 10 N/m^2 or 0.010 kPa

This experiment lasted 10 minutes with the discharge = 0.002 m^3/s and water depth on the crest = 10 mm, 10 minutes with the discharge of 0.0048 m^3/s and water depth on the crest = 20 mm, 10 minutes with the discharge = 0.0065 m^3/s and the water depth = 30 mm on the crest. After 1 minute with the water depth = 40 mm on the crest, the blocks on the downstream started to overturn and the water flow found its way below the geotextile on the upstream side of the embankment. The failure began on the upstream and sides of the channel close to glass walls.

Next, test "M-GT-D-1-2" was conducted (as shown in Figure 4.7) with larger sand and resisted longer to the water forces compared with other finer particles (D_{50} = 0.65, 0.9 mm):

The subgrade configuration corresponding to the "M-GT-D-1-2" test consists of:

1. Bottom layer: gravel with D_{50} = 2.1 mm was placed and compacted (with the thickness of 100 mm) followed by a layer of geotextile.

2. Top layer: same grains used on the top layer (with the thickness of 50 mm) followed by another layer of geotextile and the protection layer.

The flow characteristics and failure mechanism of this test are as follows:

- Velocity on the downstream = 1.12 m/s

- Maximum discharge resulted in failure of the setup = 0.0075 m^3/s

- Shear stress = 18 N/m^2 or 0.018 kPa

This experiment lasted 10 minutes with the discharge $= 0.002$ m^3/s and water depth on the crest $= 10$ mm, 10 minutes with the discharge $0.0048 m^3/s$ and water depth on the crest $= 20$ mm, 10 minutes with the discharge $= 0.0065$ m^3/s and the water depth $= 30$ mm on the crest. The experiment continued and after 4 minutes with the water depth $= 50$ mm on the crest, the blocks on the downstream overturned and the water flow found its way below the geotextile on the upstream side of the embankment. The trapped water could not find a way to get drained through the layer of soil and failure began on the upstream and sides of the channel close to glass walls.

Test 4.7 shows the experiment with the ACBs on the 14-degree slope. It is clear that placing the layer of interconnected blocks makes the embankment more stable preventing it from sudden failure. When the maximum discharge reached 0.0075 m^3/s, the blocks on the downstream overturned and sediment transport initiated. The circles and arrows on the downstream and the upstream of the embankment respectively show the block overturning and water penetration below the geotextile on the crest.

a)

b)

c)

d)
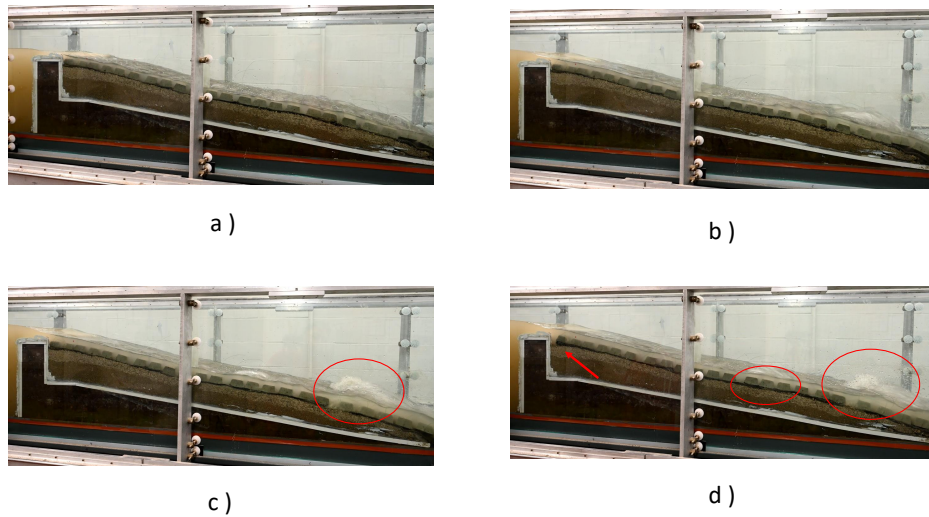
Figure 4.7: Test M-GT-D-1-2 at different stages: (a) 10 minutes with water depth $= 10$ mm; (b) 10 minutes with water depth $= 20$ mm; (c) 10 minutes with water depth $= 30$ mm on the crest; (d) when the water depth reached 50 mm on the crest, the blocks on the downstream overturned and water penetrated below the geotextile on the upstream

In test "M-GT-E-1-2", soil with the $D_{50} = 2.1$ mm was used for the bottom layer (with the thickness of 100 mm), and gravel E ($D_{50} = 3.5$ mm) was used in the setup in the top layer (with the thickness of 50 mm). Two layers of geotextile also separated the two layers and prepare the surface for the block mats as well. The setup was solid and could

resist the maximum discharge of the flume and no soil loss, sediment transport, or loss of contact of the blocks with their subgrade was observed.

The flow characteristics and failure mechanism of this test are as follows:

- Velocity on the downstream = 1.3 m/s

- Maximum discharge resulted in failure of the setup = 0.014 m^3/s

- Shear stress = 18.2 N/m^2 or 0.018 kPa

Test "M-GT-E-1-2" was conducted with the same configuration but the thickness of the top layer was lowered from 50 to 25 mm (test "M-GT-E-1-5") and the setup was stable and failure did not happen. Hence, this experiment can be considered as one of the optimal configurations with the minimum amount of gravel and the least amount of soil loss.

4.1.2 Tests on the 26.6-degree slope

In the setup with the 26.6-degree slope, test "S-GT-D-1-2" with fine sand failed with the minimum discharge. After 1 minute, the soil loss simultaneously occurred on the upstream, downstream, and sides of the channel close to glass walls.

The subgrade configuration corresponding to the "S-GT-D-1-2" test consists of:

1. Gravel with D_{50} = 2.1 mm was placed and compacted on the bottom layer (with the thickness of 100 mm), followed by a layer of geotextile

2. On the top layer, gravel with the D_{50} = 2.1 mm was placed (with the thickness of 50 mm) followed by a layer of geotextile and the protection layer.

The hydraulic characteristics of this test and the same configuration with soil B and C are as follows:

- Velocity on the downstream = 0.9 m/s

69

- Maximum discharge resulted in failure of the setup = 0.002 m^3/s

- Shear stress = 9 N/m^2 or 0.009 kPa

Having conducted different configurations on the 26.6-degree slope, finer materials could not resist the water flow forces due to the higher velocity on the downstream. Coarser gravel was used in some tests with the 26.6-degree slope using both geotextile and geogrid. Tests with geogrid could not be used with soil B, C, and D due to the larger mesh size of the fabric as the water could penetrate below the fabric and wash the materials away. On the other hand, coarser particles showed better results when geogrid was used compared with the tests when geotextile was used with larger gravel. Hence, coarser gravel on a steep slope was implemented using geogrid. The setup configuration with the 26.6-degree slope, "S-GD-E-1-2", is as follows:

1. Gravel with D_{50} = 2.1 mm was placed and compacted on the bottom layer (with the thickness of 100 mm), followed by a layer of geotextile.

2. On the top layer, gravel with the D_{50} = 3.5 mm was placed (with the thickness of 50 mm) followed by a layer of geogrid and the protection layer.

The hydraulic characteristics of this test and the same configuration with soil B and C are as follows:

- Velocity on the downstream = 1.68 m/s

- Maximum discharge resulted in failure of the setup = 0.014 m^3/s

- Shear stress = 22 N/m^2 or 0.022 kPa

This experiment continued for 10 minutes with the discharge = 0.002 m^3/s and water depth = 10 mm on the crest, 10 minutes with the discharge 0.0048 m^3/s and water depth = 20 mm on the crest, 10 minutes with the discharge = 0.0065 m^3/s and the water depth = 30 mm on the crest. This setup could finally resist the maximum discharge (0.014 m^3/s) and did not fail and no soil loss or any movement of the blocks was observed.
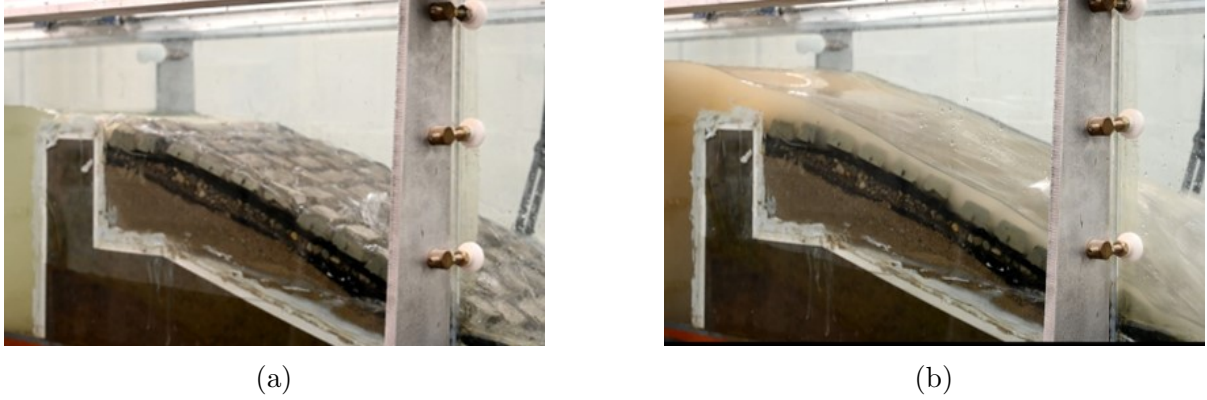
| (a) | (b) |

Figure 4.8: Test S-GD-E-1-5 at different stages: (a) water depth = 10 mm on the crest; (b) water depth = 70 mm on the crest

Test "S-GD-E-1-5" (Figure 4.8) was similar to test "S-GD-E-1-5" except for the thickness of the layers. This experiment was done due to minimizing the amount of limestone. The thickness of the bottom layer in this setup was 125 mm and the thickness of the top layer was 25 mm. This setup was also remained stable and did not fail. This configuration can be considered as the optimal configuration for 26.6-degree slope.

4.1.3 Tests with trench

As finer particles could not resist the water flow on the steep slope, another setup with the trench in between was designed. Gravel with D_{50} = 2.1 mm was placed and compacted on the bottom layer(with the thickness of 100 mm), followed by a layer of geotextile, and on the top layer, gravel with the D_{50} = 3.5 mm was placed (with the thickness of 50 *mm*) on the sides and upstream side of the embankment: polymeric sand was placed on the downstream to stabilize this vulnerable section. On the top layer, the trench was filled with angular sand D and was covered and supported with the gravel E on the sides. Plastic PVC Tubing Hose-pipe with holes pointing down into the gravel was placed around the setup to make a drainage system and help the setup to drain more water to the downstream as shown in 3.16 step (e). Movement of the blocks and soil loss was observed when the discharge reached 0.010 *m³/s* and velocity was 1.5 *m/s* on the downstream. The erosion happened on the downstream section and the polymeric sand was completely washed down.

Test "Trench 2" followed the same procedure. In this experiment gravel with the D_{50} = 3.5 mm was used on the sides and downstream as well and remained stable without any movement or deformation of the blocks. The same configuration was used in the test "Trench 3" but the thickness of the gravel was lowered by half to minimize the amount of

the limestone, which could resist the maximum discharge and the failure threshold was not met. The drainage system can be seen in Figure 4.9.
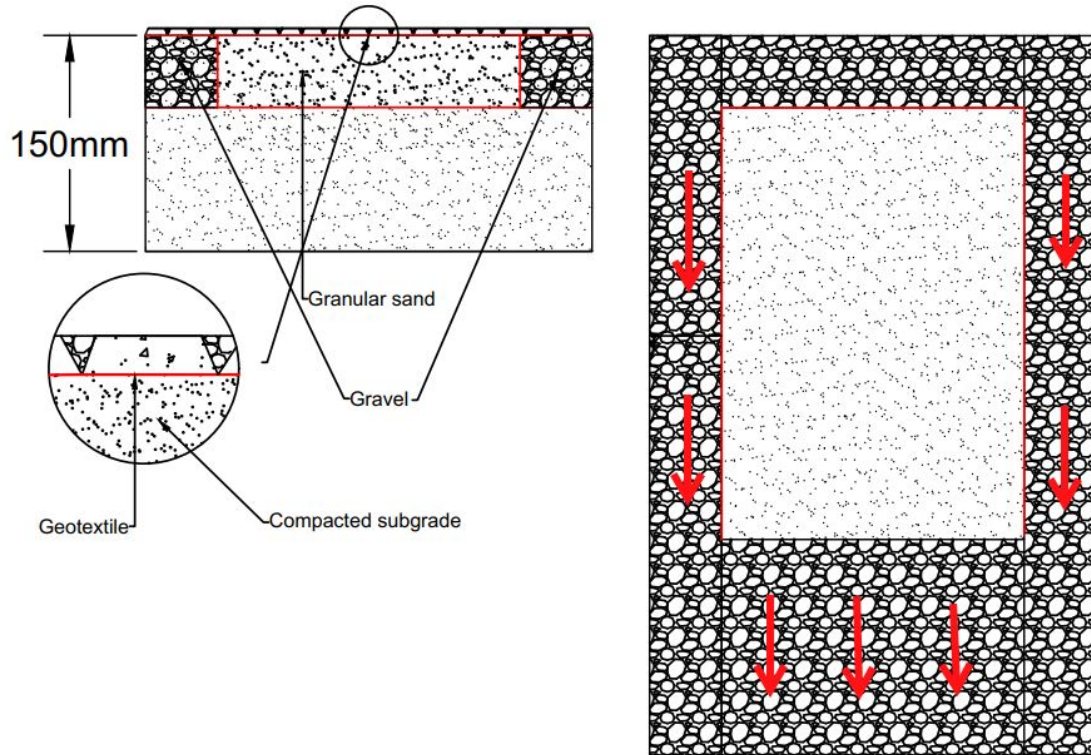

Figure 4.9: Plan of the Trench

Table 4.2 presents the results for the selected experiments out of the ~ 40 tests with the protective layer (see 4.1.1 and Table 3.6).

Table 4.2: Summary of the parameters considered in the experiments with ACBs. Q: Maximum Discharge; V: Maximum velocity; δ: Soil loss

Experiments	Q (m^3/s)	V (m/s)	δ (%)
M-GT-B-1-2	0.0048	0.91	20
M-GT-C-1-2	0.0048	0.91	15
M-GT-D-1-2	0.0085	1.12	10
M-GD-E-1-2	0.014	1.3	0.2
M-GD-E-1-5	0.014	1.3	0.2
S-GT-B-1-2	0.002	0.90	75
S-GT-C-1-2	0.002	0.90	60
S-GT-D-1-2	0.002	0.90	40
S-GT-E-1-2	0.014	1.68	1
S-GT-F-1-2	0.014	1.68	0.7
S-GD-E-1-2	0.014	1.68	0.8
S-GD-F-1-2	0.014	1.68	0.2
S-GD-E-1-5	0.014	1.68	0.8
S-GD-F-1-5	0.014	1.68	0.2
Trench 1	0.010	1.48	5
Trench 2	0.014	1.68	2
Trench 3	0.014	1.68	2

4.1.4 Locations of failure

Figures 4.10 and 4.11 show the soil loss at different locations along the embankment for the 14-degree and 26.6-degree slopes. Erosion shows an increasing trend over time but the point being is that distance of the soil loss from the toe of the embankment considerably proceeded as the sediment transport initiated and it gradually grew after it reached a certain point. As an example, the slope of the soil loss-distance increasing curve for the soil D, after 20 mm from the toe on the 14-degree slope, decreases and slightly continues to grow until the system fails. Overall, a clear upward trend can be seen in the graphs for both slopes, and the distance was proceeding on the steeper slope and growing faster. Figure 4.11 shows the distance from the front edge of the embankment for the 26.6-degree slope. Having used sand on the steep slope, the soil loss trend shows a significant increase and it continues to grow until the setup fails. The gravel does not show any difference in the location of the failure for both slopes.
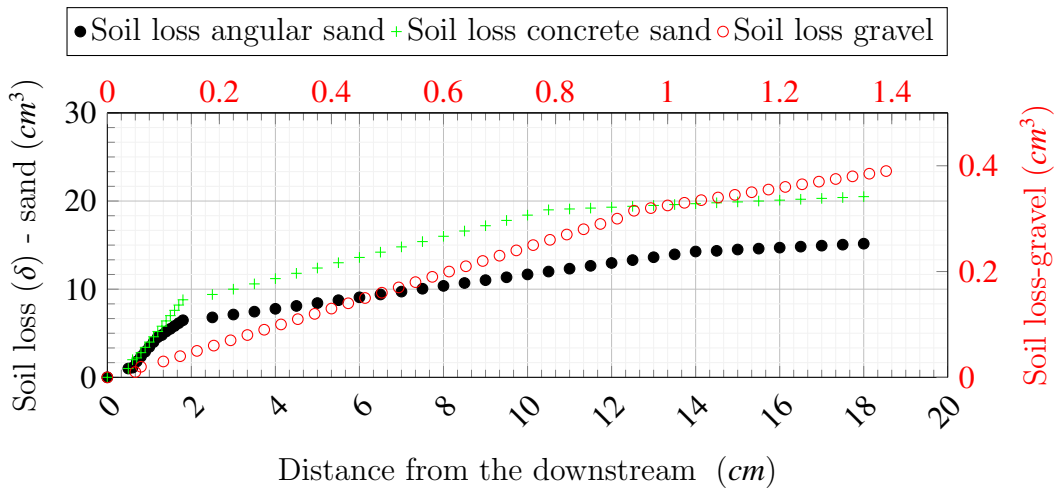
Figure 4.10: Soil loss-Distance from the toe of the embankment on the 14-degree slope
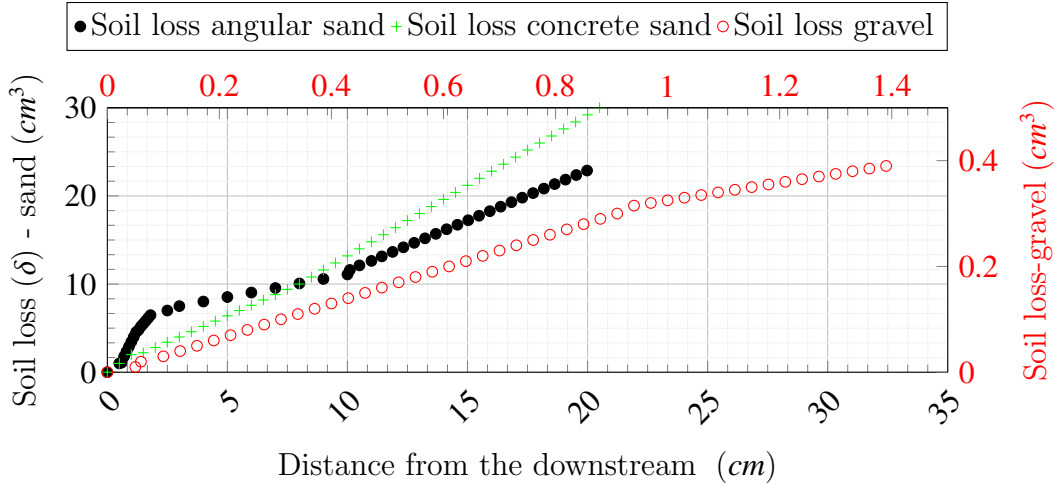
Figure 4.11: Soil loss-Distance from the toe of the embankment on the 26.6-degree slope

4.1.5 Time of Failures

Figure 4.12 presents the time of the embankment's deformation for the 26.6-degree slope. Erosion showed to be advanced over time. The point being is, the sediment transport rate increased sharply in the first period of each experiment and grew steadily after this period until the failure of the blocks happened.

Figure 4.12: Soil loss (cm^3) - Time (min)

Figure 4.13: Forces on the blocks

4.1.6 Block Failure

Water Flow Forces

Higher velocity and the corresponding shear stress, as well as the uplift force, can move the blocks. Figure 4.13 shows the block movement in the horizontal and vertical direction due to higher velocity and uplift forces respectively as a result of the direct 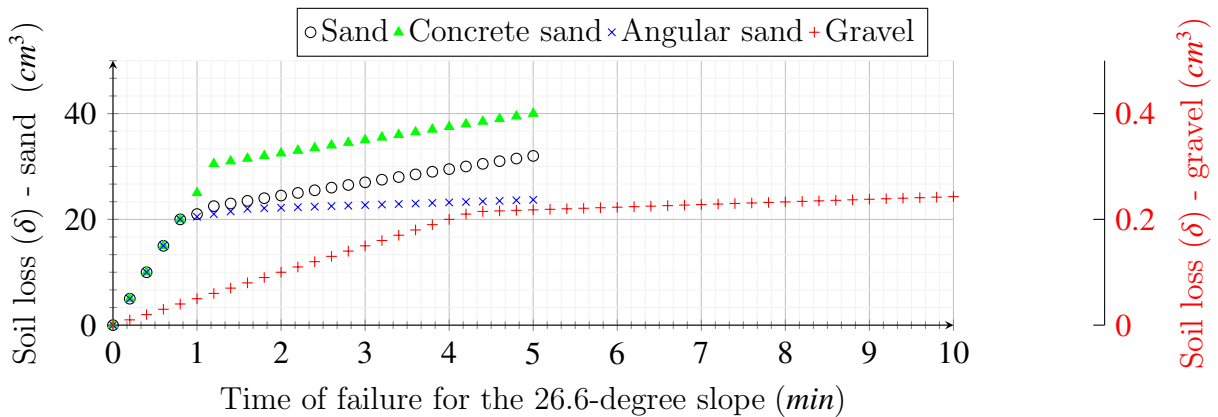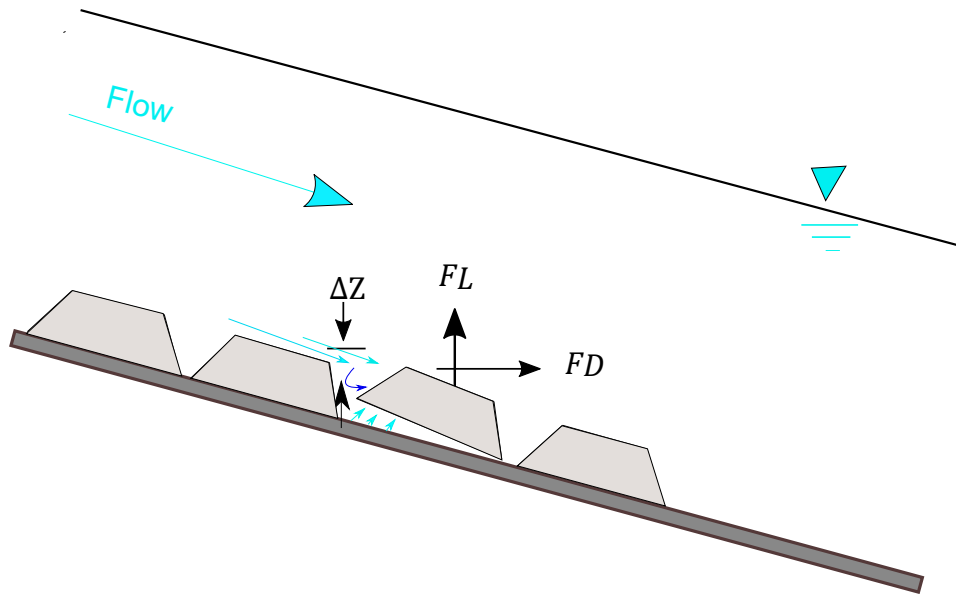effect of water flow forces. In addition to the direct effect of the water flow, the bedding effect which was the main focus of this study was investigated. In the experiments with coarser gravel, water is drained through the larger void between the grains, and higher hydraulic conductivity of the gravel E and F causes the drainage to happen and helps the embankment to remain stable. Hence, there is no significant uplift force upon the blocks from the subgrade. In the experiments with finer materials, water was trapped in between the grains and cannot find a way to be drained and it makes a force on the blocks. Figure 4.14 (b) shows another form of block failure which happens when the blocks lose contact with their subgrade. When losing contact with subgrade, the blocks are more vulnerable to be moved, overturned, and let more water pass through them and displace them. In addition, when the blocks lose their contact with the fabrics and the subgrade, the system is not working properly and sediments are being exposed to water flow and are more likely to be eroded.

(a) Overturning

(b) Loss of contact

Figure 4.14: Blocks failures

Bedding Failure

High velocity, increased bed shear stress, turbulent flow on the landward side of the embankment, and soil characteristics according to different configurations play a key role in scouring on the embankment. In the presence of sand layers, the erosion starts at the toe of the embankment, expanding towards the upstream, until the system fails. Figure 4.15 (c) shows the soil loss on the bottom layer after the test when the soil used on the top layer was fine sand. Based on the experiments conducted in the lab for both 14 and 26.6-degree slopes, failures and vulnerabilities are initiated on the sides and the edges of the embankment. Horseshoe-shaped vortices can be generated due to the erosive action of the water flow; these vortices grow on the sides and edges of the setup continuously, until it reaches the maximum depth of the soil layers and fails the setup. Figure 4.15 illustrates the erosive action of the water flow in the mentioned segments. Compaction is another issue which results in stabilizing the embankment. Figure 4.16 (a) shows the configuration of one experiment with angular sand with $D_{50} = 2.1$ mm on the bottom and gravel with $D_{50} = 3.5$ mm on the top followed by a layer of geogrid. After 10 minutes with the maximum discharge ($0.014\ m^3/s$) the test was stopped and the ACB mat and the top layer were removed to analyze the amount of soil loss happened in the experiment. Figure 4.16 (b) the importance of the compaction of the soil on the downstream side of the embankment. If the soil is not well-compacted, the toe of the embankment can be more vulnerable to scouring as this area is more exposed to the higher shear stress.
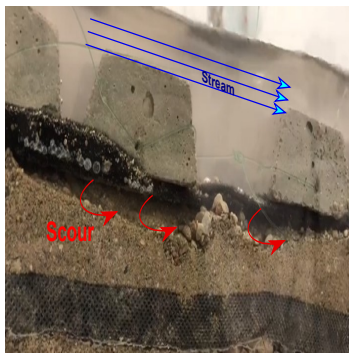
(a) Vortices on the sides

(b) Loss of contact on the upstream

(c) Scouring

Figure 4.15: Bedding failures

(a)

(b)

Figure 4.16: (a) Side view of the test with the subgrade non-compacted; (b) Soil loss as the result of lack of compacting the subgrade

Figures 4.17 and 4.18 show the water velocity, and the percentage of soil loss according to the median diameter in different experiments for both 14 and 26.6-degree slopes. According to the graphs, the percentage of the soil loss in the 26.6-degree slope is higher than that for the 14-degree slope and it gets to less than 1 % for both slopes when gravel is used.
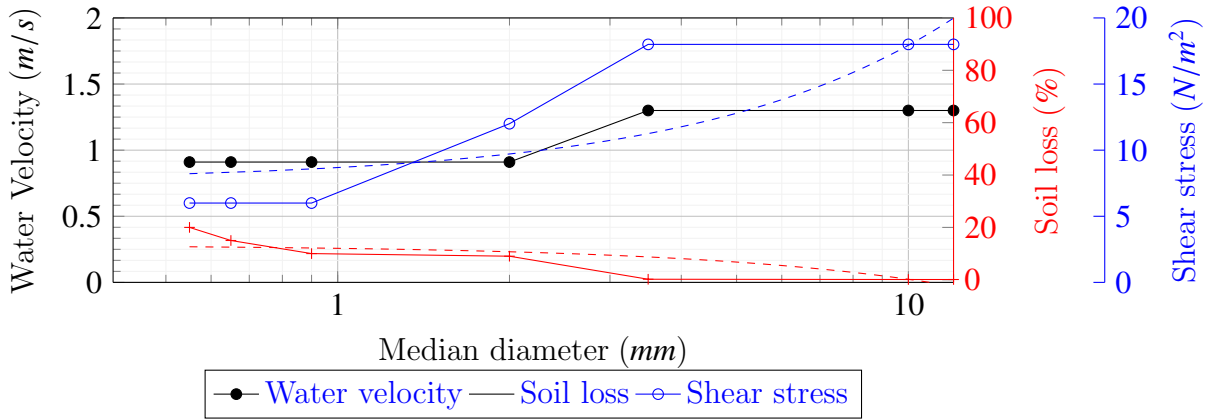
Figure 4.17: Water velocity, shear stress, and soil loss in each test for 14-degree slope
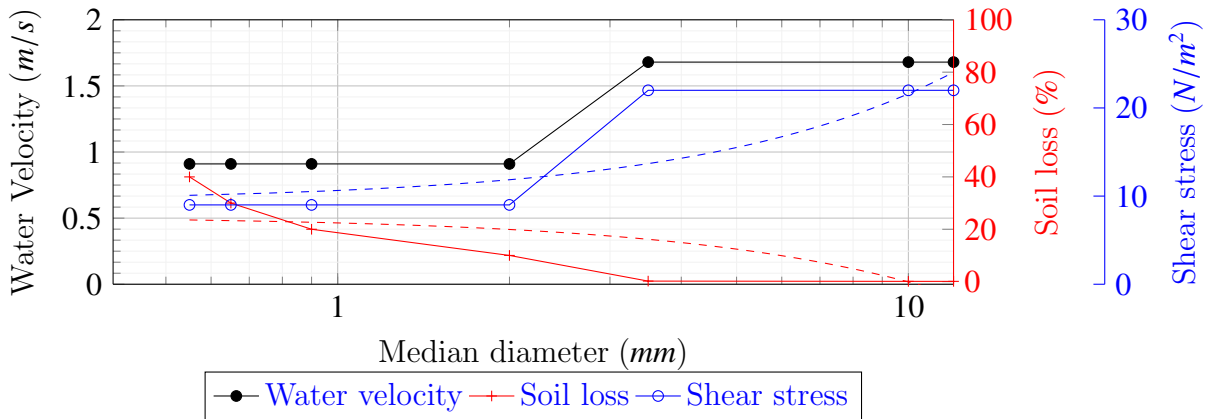
Figure 4.18: Water velocity, shear stress, and soil loss in each test for 26.6-degree slope

4.2 Conclusions

9 experiments without the protective ACB layer and 31 tests with ACBs, considering various designs and subgrade configurations, were conducted in the hydraulics lab. The results suggest that:

- Angular grains with larger voids in between the particles showed to be more resistant against the local scour.

- The median diameter of the particles showed that the size of the grains used in the tests is the main variable that contributes to the stability of the embankment.

- Some systems such as trench setup can be considered to minimize the amount

of limestone used in each project. The trench system remains stable as it covers the vulnerable segments and can drain the water downstream. This will reduce the uplift force on the concrete blocks, hence, Articulated Concrete Blocks remain stable on the embankment.

- Scour increases significantly at the beginning of each test and it gradually increases after a certain amount of time.

- Location of the failures are mostly on the toe, sides, and upstream side of the setup and these sections need extra care.

- According to the effect of the variables, water depth, and grain size were the leading variables in scouring and its control. The thickness of the layer showed the minimum effect on the failure of the embankment. The reason is that if the soil used as the layer is gravel, the water passes through the voids with the minimum thickness (25 mm recommended) and if the finer particles are used, a large amount of the layer would be eroded particularly on the 26.6 degrees.

- Experiments with the ACBs with 2 blocks extended to the bottom of the flume as well as blocks attached to the upstream showed that indirect failure took longer to happen. Furthermore, toe support conditions were found to have effects on the failure mechanism and the overall stability of the placed protective layer.

- Using a high permeable filter between the layer and underneath the concrete blocks may cause the water trapped in between the particles and cause weakening and failure of the setup.

- To decrease the erodability of the experiment, compaction of the soil is to be done based on the ASTM standards and procedures. On the condition that the soil is noncompacted, there would be more amount of soil loss on the toe of the embankment.

Bibliography

Rai, R. K., Singh, V. P., and Upadhyay, A. (2017). Chapter 2 - irrigation project planning. In Rai, R. K., Singh, V. P., and Upadhyay, A., editors, *Planning and Evaluation of Irrigation Projects*, pages 7–24. Academic Press.

Chapter 5

Conclusions and future works

Articulated Cable Concrete (ACB) can provide a wide range of solutions for soil erosion control to a variety of applications such as culvert inlet/outlet protection, dam overflow/intakes, etc. One of the main failure mechanisms of ACBs in river projects is associated with the inappropriate implementation of the subgrade and its subsequent indirect effects on the ACB mats. In this study, the stability of scaled Articulated Concrete Block systems downstream of an embankment is analyzed. 40 laboratory experiments were conducted to determine the effects of subgrade configuration underneath the protective layer and identify the optimal design.

Multiple factors can enhance or limit scouring in the open channels including flow rate and depth, the slope of the embankment, soil type and particle size, density, and the thickness of the bedding layers. Various subgrade configurations with different soil combinations were tested to analyze the indirect failure mechanisms of ACBs and determine the optimal subgrade configuration. Some of the key findings of this study are as follows:

Soil Effects

- Tests with a trench (those with gravel on the sides as well as downstream of the embankment followed by a layer of geotextile and a layer of geogrid below the ACB mat) showed the most optimal experiments with the minimum amount of soil loss. The system could drain the water downstream of the embankment through the larger voids of the gravel. In addition, geogrid used in the experiments with gravel let the water pass through its mesh.

- According to the effect of the variables, water depth, and grain size were the leading variables in scouring and its control. The thickness of the layer showed the minimum effect on the failure of the embankment. The reason is that if the soil used as the layer is gravel, the water passes through the voids with the minimum thickness (25

mm in the experiments) and if the finer particles are used, a large amount of the layer would be eroded particularly on the 26.6 degrees.

- Fine soil particles in the sublayer result in scouring of the bedding underneath the ACBs leading to the indirect failure of this protective measure. Gravel due to the higher hydraulic conductivity results in less drag on the seepage force and allows better drainage so the hydraulic gradient is reduced. This causes less seepage force and a more stable slope.

- Compaction of the bottom and the top layer is to be completely uniform, otherwise, the water flow passes through a higher gradient to a lower gradient and results in higher stress in some sections and earlier failure of the setup.

- Soil particles in the bedding can winnow out from the top layers if the layers are too thin. Minimum of 25 mm thickness of gravel for the top layer showed to be more effective in the experiments for both 14 and 26.6-degree slopes.

- When gravel was used on the top layer on both slopes, the amount of soil loss decreased to % 1, and the maximum water velocity and shear stress that the blocks can stand on the downstream increased by nearly % 40 for both slopes.

Effects of Fabrics

- When laying the blocks on the geotextile, care must be taken not to move the filter, particularly on the edges. Filters are to be overlapped and their edges are recommended to be extended over each other to prevent water penetration beneath the fabrics, otherwise, if the permeability of the filter layer is not adequate to drain the water, the subsoil is more likely to be washed out.

- Blocks are to be well attached to the filter to cover all parts of the filters. Otherwise, the materials beneath the fabrics could be easily displaced and fail the system.

- Geogrid can only be used for coarser sand and gravel, while geotextile can be used for both sand and gravel. When geotextile is laid on the sand and fine particle layer, water cannot be drained and will be confined in the layer.

- Geogrid shows more strength and stability against soil loss when used with larger stones such as gravel, compared with the geotextile.

- If the permeability of the geotextile is inadequate, or if the geotextile is clogged, the geotextile will act like a geomembrane and result in uplift under the ACBs.

Provided that the uplift force exceeds the combined weight of the surface water and ACBs above the geotextile, the ACBs will be displaced upward. Using more permeable geotextile could resolve this issue to let the water pass through the voids.

ACB Effects

- Blocks are to be in close contact with the fabrics and subgrade to help regulate and minimize sediment transport.

- Blocks are to be placed from the toe of the embankment to the upstream to avoid any tension in the interlock ropes.

- At the transition points in which the blocks are attached to the embankment, more vulnerabilities and soil loss happen.

- Downstream of the embankment is exposed to flow with relatively higher velocity and shear stress.

- The excessive spaces between the protective layer cause the overturning and direct failure of the blocks.

- Experiments with the ACBs with 2 blocks extended to the bottom of the flume as well as blocks attached to the upstream showed that indirect failure took longer to happen. Furthermore, toe support conditions were found to have effects on the failure mechanism and the overall stability of the placed protective layer.

Location and Time of failures

- A large amount of erosion happened close to the toe of the embankment and slightly continued to grow (to the upstream side of the embankment) until the system failed.

- Erosion can advance over time for both 14 and 26.6-degree slopes. The amount of erosion rises sharply in the bottom period of each experiment and grows steadily after the period until the failure of the blocks happens.

During this study there were some limitations:

- The experiments were conducted with one ACB mat for both slopes

- The glass walls of the hydraulics flume could affect the earlier soil loss on the sides.

Suggestions for Future Research

This study was focused on the indirect failure of ACBs based on a scaled model with a width of 31 cm and a height of 47cm. Future studies can focus on both direct and indirect failure mechanisms of the concrete blocks where flow directly interacts with the blocks and result in rolling up the edge of the mat or overturning the individual blocks and subsequently affecting the subgrade. Besides, larger hydraulic flumes would allow further limit the effects of side walls. Also, it is important to analyze other forms of ACBs with various types of concrete specifications and shapes. Moreover, some other indexes could be used to analyze the failure and the time of the failure of the ACB.

Appendix A

Python Function

A Python function was implemented to calculate the equations of the direct step method.

Require: $Slope(S), Manning's(n), water\,depth(H)$

Ensure: $Velocity, Shearstress, normaldepth, etc.$

   for $ls = 1 : length(s)$ **do**

      for $lh = 1 : length(H)$ **do**

         $Q \leftarrow 1.627b(H[lh]^{3/2})$

         $y_c \leftarrow \frac{2}{3}H[lh]$

         $Q \leftarrow sqrtgY_c^3$

         $A \leftarrow by_c$

         $P \leftarrow (Y_c * 2) + b$

         $Y_n \leftarrow solve((1/n) * (b * x) * (((b * x)/(b + 2 * x))^{2/3}) * ((S[ls])^{0.5}) - Q, x)$

         $y \leftarrow y_c : -0.001 : Y_n$

         while $y[i]notempty :$ **do**

            $area[i] = y[i] * b$

            $V[i] = Q/area[i]$

            $p[i] = b + 2 * y[i]$

            $r[i] = area[i]/p[i]$

            $e[i] = y[i] + ((v[i]^2/(2 * 9.81))$

            $se1[i] = ((v1[i]^2) * (n^2))/r1[i]^{(4/3)}$

            $f1[i] = (v1[i])/np.math.sqrt(9.81 * y[i])$

            $sebar[i] = (se1[i] + se1[i - 1])/2$

            $DE[i] = e2[i] - e2[i - 1]$

            $DX[i] = DE[i]/(S[ls] - sebar[i])$

$i + +$

$data = [y, Area, velocity, shear stress, ...]$

end while

end for

end for

return data

Appendix B

Block Rotation

Figure B.1 shows the block rotation when the driving forces are larger than the resistance forces of the blocks. The loss of intimate contact occurs when the blocks are being overturned due to both hydraulic causes(such as volume of the flow higher than overturning moments and resistant force of the blocks) and subgrade reasons (when inappropriate soil and subgrade is used). The hydraulic stability of a block depends on block weight and interconnect force which connects the blocks with each other (called restraining forces) and hydrodynamic drag and lift forces (Overturning forces). The safety factor is a ratio which can be considered in designing the blocks (Cox et al., 2014).

$$SF = \frac{l_2 W_2 \alpha_\theta}{l_1 W_s \sqrt{1 - \alpha_\theta^2} \cos\beta + l_3 F_D \cos\delta + l_4 F_l + l_3 F'_D \cos\delta + l_4 F'_l} \tag{B.1}$$

W_s is the weight of the block; l_1, l_2, l_3, and l_4 are the moment arms.
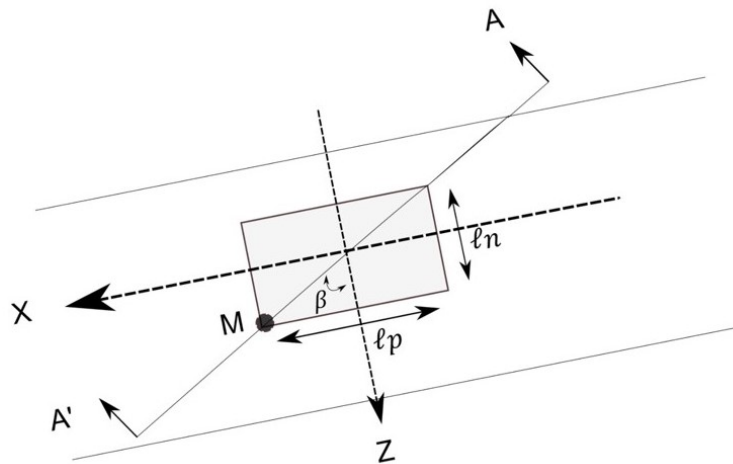

Figure B.1: Block rotation

Before the slope failure of the particles because of high discharge happens, some individual particles start moving the downstream and this is happening due to the overturning moments which are the drag, lift, and buoyancy forces that surpass the resisting moments.

BIBLIOGRAPHY

A. L. Cox, C. I. Thornton, and S. R. Abt. Articulated concrete block stability assessment for embankment-overtopping conditions. *Journal of Hydraulic Engineering*, 140(5): 06014007, 2014.

You may see the link below to see some of the videos and photographs of the experiments

Thesis

Curriculum Vitae

OMID MARANDI

EDUCATION

PERIOD	**January 2020 — February 2022**	
DEGREE	**Master of Science in Civil and Environmental Engineering**	
UNIVERSITY	**Western University**	London, Ontario, Canada

PERIOD	**October 2010 — September 2014**	
DEGREE	**Bachelor of Civil Engineering**	
UNIVERSITY	**Esfahan Azad University**	Esfahan, Iran

SKILLS

Programming Languages	Python, MATLAB, R
Modeling Software	ArcGIS, HEC-RAS, HEC-HMS, SWMM, Ansys Fluent, GeoStudio
Designing Software	AutoCAD, AutoCAD Civil 3D

ACADEMIC PRESENTATIONS

Marandi M.O, Najafi M.R, Mohajeri S.H, Attari J, Sadrekarimi A, Ahmed A, Newson T. "Erosion Control of Steep Open Channels Using Articulated Concrete Blocks". Poster virtualy presented at: 2021 Fall meeting, AGU Conference; New Orleans 13-17 Dec.

Rahimimovaghar M, Rezvani R, Marandi M.O, Najafi M.R. "Spatial and Temporal Characteristics of Compound Dry and Wet Spells across Canada". Poster virtualy presented at: 2021 Fall meeting, AGU Conference; New Orleans 13-17 Dec.